UNIVERSITY OF OKLAHOMA

GRADUATE COLLEGE

THE KEROGEN 3D SOLID STATE STRUCTURE MODELING AND ITS APPLICATIONS IN RESERVOIR SIMULATION

A THESIS

SUBMITTED TO THE GRADUATE FACULTY

in partial fulfillment of the requirements for the

Degree of

MASTER OF SCIENCE

By

ZHENYU ZHANG
Norman, Oklahoma
2016

THE KEROGEN 3D SOLID STATE STRUCTURE MODELING AND ITS APPLICATIONS IN RESERVOIR SIMULATION

A THESIS APPROVED FOR THE
MEWBOURNE SCHOOL OF PETROLEUM AND GEOLOGICAL ENGIEERING

BY

_____
Dr. Ahmad Jamili, Chair

_____
Dr. Xingru Wu

_____
Dr. Bor-Jier Shiau

Dedicated to my family and my friends

Acknowledgements

First and the most, I would like to express my heartiest gratitude to my academic advisor, Dr. Ahmad Jamili. Without his kind support, it would have been impossible for me to work in the areas of petroleum engineering and mathematic modeling. His patient guidance is the most valuable treasures in my petroleum engineering study.

I would like to thank Dr. Xingru Wu and Dr. Bor-Jier Shiau, the members of my thesis committee for shaping the course of my graduate program. I greatly appreciate their time in reviewing this work and making valuable suggestions and comments.

I would also like to thank Dr. Carl Sondergeld and Dr. Chandra Rai for allowing me to participate in the Unconventional Shale Resource Consortium during my first year, which greatly extended my knowledge in petrophysics.

Finally, I would like to thank my family for their constant support to me, which is always my biggest driving force. Also I would like to have special thanks to my labmates and classmates at OU, especially Luchao Jin, Yixin Ma, Felipe Perez, Binbin Mu, Lianbo Hu, Wei Tian, Jiman Liu, and many others who helped me through the hard time in my classes and research.

Table of Contents

List of Tables

List of Figures

Abstract

A 3D solid state Green River Oil Shale kerogen model was built in this thesis through the following two steps: 1. a molecular nanocluster model of kerogen composed of seven molecules was built based on an adsorption method; 2. the molecular nanocluster model was further transformed into a solid state model based on molecular dynamics simulation method. Moreover, with this 3D solid state model, a porous solid state kerogen model was further proposed based on the formation mechanism of the nanopores in kerogen.

Based on the solid state 3D model of kerogen, some physical, chemical and mechanical properties of the kerogen, such as density, Young's modulus, Poisson ratio, compressibility, bulk modulus and shear modulus, IR, Raman, ^{13}C and ^{1}H spectra were calculated using quantum chemistry or molecular dynamical simulation methods. The theoretical calculation results matched the reported experimental results very well. Moreover, based on the porous model of kerogen, the sorption isotherms of six alkane gas molecules from methane to hexane at 212^{o}F were calculated and it was discovered that the adsorption could be described by Langmuir model very well. Two empirical equations were established to calculate the parameters of Langmuir model. All the theoretical calculation results matched the reported experimental results very well.

These proposed method established a way to study and understand the properties of kerogen theoretically which provides the opportunities to extract the parameters for hydraulic fracturing design and reservoir simulation based on computational chemistry methods. The developed methods in this thesis can be further applied for other kerogen

samples and may find wild applications in implementing new techniques or improving existing methods for hydraulic fracturing and enhancing oil recovery for shale resources.

Chapter 1: Introduction

1.1 The Demand for Kerogen Modeling

The last decade has witnessed the surge and prosperity of the recovery of unconventional resources, such as shale oil and gas. In May 2015, the weekly crude oil production in U.S. ascended to a record high level of 9.56 million barrels per day due to the continuous increase of shale oil production. At the same time, the Marcellus shale play alone was contributing more than 18% of the total U.S. dry gas production. Predictably, shale gas and oil will play an even more important role in the energy industry in the near future. Therefore, great research efforts have been conducted to tackle the problems in shale reservoir recovery.

Currently one major challenge in shale oil recovery is the low recovery factors less than 10%. Therefore, effective methods to improve oil recovery factor are highly desired. In our opinion, understanding the structure and properties of kerogen is the basis for developing such methods. Firstly, it is well accepted that both natural gas and oil are generated from kerogen. Therefore, the kerogen model is of great importance to understanding the oil/gas generation process. Secondly, in shale reservoirs, more than as the source of hydrocarbons, kerogen also plays a key role in adsorption, storage and migration of hydrocarbons. Thirdly, in shale plays the hydrocarbons can be recovered economically only through horizontal drilling and multi-stage hydraulic fracturing. To optimize hydraulic fracturing design for higher recovery factors, it is crucial to understand the mechanical properties of shale, a heterogeneous composite material. An essential component of shale, the source rock, is kerogen, which is the source of oil and

gas. Therefore, it is vital to theoretically understand the structure and mechanical properties of kerogen and further explore their impacts on the mechanical properties of shale.

In addition, another important way for shale oil production is shale oil extraction during which shale oil is produced by pyrolysis, hydrogenation, or thermal dissolution reaction of kerogen. The basis of the optimization of reaction conditions and production yield enhancement is the clarification of the structure and properties of the reactant: kerogen.

1.2 Objective of This Study

Due to the importance of 3D kerogen model in petroleum industry, in this thesis, the following goals will be achieved:

1. Although kerogen is a mixture of multiple molecules, there was only one single macromolecule in most of current kerogen models which may be because of the lack of suitable techniques to combine various molecules together. Therefore, the first objective of this thesis is to develop a method to assemble several molecules together to build a molecular nanocluster model of kerogen which is a mixture not a single macromolecule;
2. With only a single macromolecule, most current kerogen models were not real solid state materials. The molecular nanocluster model constructed in the first step of this thesis is also not a solid state material model. Therefore, the next objective of this thesis is to develop a method to transform the molecular nanocluster model into a solid state model of kerogen;

3. With the 3D solid state kerogen model as the basis, the third objective is to calculate the mechanical properties and spectral properties of kerogen based on quantum chemistry methods and MD simulation methods. The comparison of our theoretical results with previously reported experimental results will provide the best way to justify our proposed methods to build the model and the validity of the model itself;
4. Adsorption plays a key role in the storage and recovery of shale gas. A porous kerogen model is the key to study the adsorption and transportation of hydrocarbons in shale reservoirs. The fourth objective of present thesis is to figure out a method to build a porous kerogen model. Moreover, the adsorption properties of alkanes on the porous kerogen will be studied theoretically and the results will be applied into a shale gas reservoir simulation.

1. 3 Outline of This Thesis

The following is an outline and brief description of the remainder this thesis:

Chapter II contains a literature review about the formation of kerogen and oil/gas, potential applications of kerogen models in petroleum industry and current status of 2D/3D kerogen modeling;

Chapter III introduces the theoretical basis of quantum chemistry and MD simulation used in the present thesis;

Chapter IV elucidates our proposed methods to build up a 3D solid state kerogen model and reports the mechanical properties and spectral properties calculated theoretically based on the 3D solid state model;

Chapter V elucidates our method to construct a porous kerogen model from the 3D solid state kerogen model. Moreover, the adsorption of hydrocarbons on the porous model is calculated and applied in a shale gas reservoir simulation.

Chapter VI includes conclusions that can be drawn from the results presented in previous chapter, as well as recommendations for further studies.

Chapter 2: Literature Review

In this chapter, the formation of kerogen, oil and gas, the potential applications of kerogen model and previous literature related to kerogen modeling will be introduced.

3. 1 Diagenesis and Formation of Kerogen

Upon the death of living beings, such as planktons, spores and diatoms, if they are isolated from oxygen at the deep bottom of oceans/lakes, these organic matters will be mixed with sand/mud, buried underground and become part of sediment. In aquatic environments, the biopolymers are decomposed by microbial action into smaller compounds. Then these constituents undergo new condensation reactions and produce fulvic acids and humic substances which become progressively insoluble due to increasing polycondensation and finally result in kerogen. This process is termed diagenesis, which can be viewed as a process through which the system approaches equilibrium under the shallow burial conditions.

Kerogen is a mixture of organic compounds from which hydrocarbons were generated with increasing burial, pressures and temperatures. Kerogen is insoluble in organic solvents due to the high molecular weight of its component compounds. Traditionally, there are three general types of kerogen: types I, II and III. Occasionally a type IV kerogen is also recognized which has extremely low H and O contents. The characteristics and differences between the type I, II and III kerogen can be best illustrated by a Van Krevelen diagram[1] as shown in Fig. 2.1.

As shown in the Van Krevelen diagram, for type I kerogen, the hydrogen:carbon ratio is larger than 1.25 and oxygen:carbon ratio is less than 0.15. It is assumed that type I kerogen originated mainly from lacustrine algae and formed only in anoxic lakes and several other unusual marine environments. Few cyclic or aromatic structures exist in type I kerogen and there is a great tendency for type I kerogen to produce liquid hydrocarbons. More volatile or extractable compounds can be obtained from type I kerogen than any other types during pyrolysis. Therefore, theoretically Type I kerogen oil shales should provide the highest yield of oil and are the most commercially promising deposits using conventional oil retorting techniques.

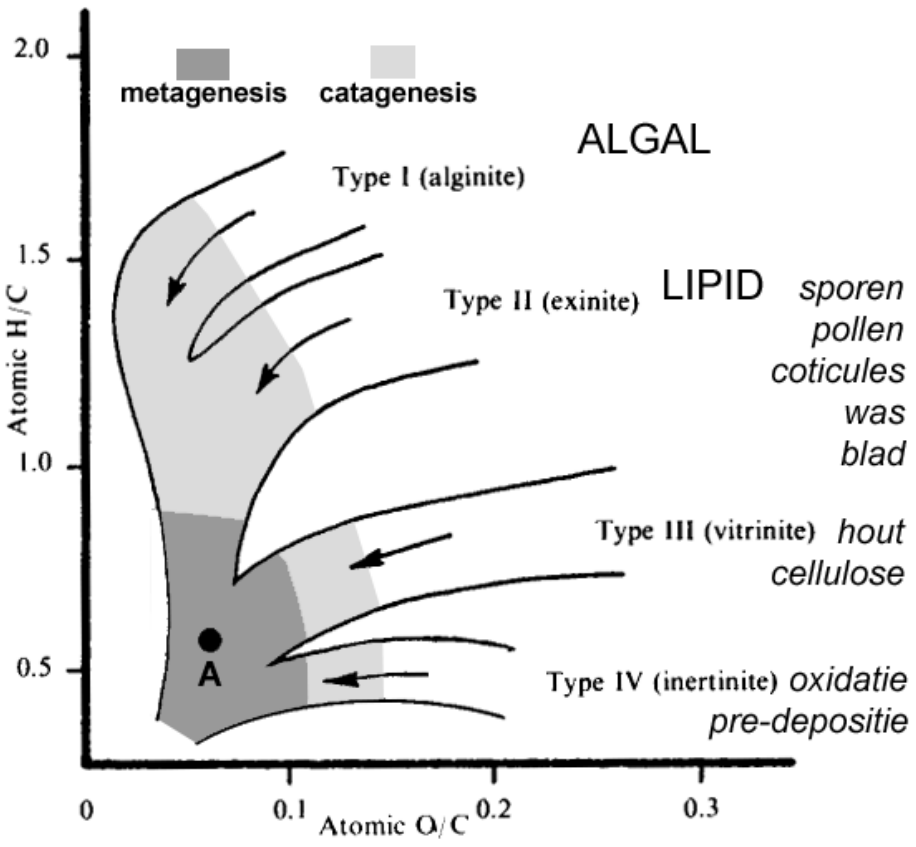

Figure 2.1 Van Krevelen diagram

(http://alfonsussimalango.blogspot.com/2011/10/diagram-van-krevelen.html)

For type II kerogen, the hydrogen:carbon ratio is less than 1.25 and oxygen:carbon ratio is between 0.03 to 0.18. This type of kerogen tends to produce a mixture of gas and oil. This type of kerogen is originated from marine organic materials that are also formed in reducing environments. For type III kerogen, the hydrogen:carbon ratio is less than 1 and oxygen:carbon ratio is between 0.03 to 0.3. This type of kerogen tends to produce a mixture of gas and oil. Type III kerogen is originated mainly from terrestrial plant matters. There exist extensive ring and aromatic systems in this type of kerogen. Hence, upon pyrolysis, only coal and gas will be produced. The hydrogen: carbon ratio of Type IV kerogen is less than 0.5. The organic matters in this type of kerogen are mostly in the form of polycyclic aromatic hydrocarbons. There is no potential for this type of kerogen to produce hydrocarbons.

3.2 Catagenesis, Metagenesis and Formation of Oil and Gas from Kerogen

Consecutive deposition of sediments induces burial of previous beds deeper, the equilibrium established at the end of diagenesis to form kerogen is broken by increasing temperature and pressure. The sedimentary evolution enters the stage of catagenesis. The temperature of this stage ranges from 50 to 150^{o}C and the pressure varies from 300 to 1500 bars. For inorganic materials, the rocks are further compacted and water is further expelled. As a result, porosity and permeability of sediments decrease significantly in this stage. For organic materials, the higher temperature and pressure induce the decomposition reaction of kerogen. Initially, liquid black oil is produced and then in the later stages volatile oil, condensate, wet gas and dry gas are produced in sequence at higher temperatures. At the end of catagenesis, all the aliphatic carbon chains in kerogen disappear and there is no more generation of petroleum from kerogen.

The following stage is metagenesis. At this stage, organic matter is composed only of methane and a carbon residue. Only methane can be produced at this stage from further decomposition of kerogen. Normally the temperature at this stage ranges from 150 to 200^{o}C.

3.3 Applications of kerogen model in understanding Oil and Gas Formation

As discussed above, modern geochemistry research indicates that all the oil and gas are produced from kerogen. The formation process of oil and gas is in fact a thermal decomposition reaction of kerogen at certain temperatures and pressures. To understand a chemical reaction, the most important concern is the 3D molecular structures of the reactants. Based on the advanced techniques of the modern computation chemistry, once a 3D molecule structure model of a reactant is available, in principle all the following thermal decomposition processes can be predicted theoretically. Therefore, it is of great importance to clarify the 3D molecular structure of kerogen.

3.4 Applications of kerogen model in oil shale production

As discussed above, petroleum can be produced from kerogen as a natural geological process which is very slow and may take millions of years. To match the current global oil demand, one of the most promising alternative methods to obtain oil is to extract oil by direct artificial thermal decomposition of kerogen in the source rocks. A major concern about commercial application of the oil shale extraction techniques is cost. The cost of oil derived from oil shale is significantly higher than that of oil from conventional reservoirs.

For future development of oil shale industry, it is urgent to find out the methods to reduce the cost of oil shale extraction techniques. The kerogen decomposition is essentially a chemical reaction process. To find out a way to optimize the conditions and improve the yield for a chemical reaction, the most indispensable and crucial step is to figure out the composition and structure of the reactant. There is no doubt that a reasonable 3D structure model of kerogen will provide a solid theoretical basis for the future development of the oil shale industry.

3.5 Applications of kerogen model in shale gas/oil recovery

Apart from oil shale industry, the structure model of kerogen will play a vital role in shale gas and oil recovery, from hydraulic fracturing design to enhanced shale oil/gas recovery (EOR).

Kerogen model is of great importance for shale play recovery. Kerogen is an indispensable component of shale. Therefore, different from conventional reservoirs, all the techniques to recover oil/gas from source rocks will be inevitably related to the properties of kerogen.

First of all, the recovery of shale oil/gas is dependent on the hydraulic fracturing techniques that the hydraulic fracturing design is based on mechanical properties of shale. As a composite material, the mechanical properties of shale are determined by the mechanical properties of its components: inorganic minerals, such as clay, quartz, carbonates and organic components such as kerogen. There is no doubt that the central goal of hydraulic fracturing is to make artificial fractures reach and connect the kergogen-rich pores or the microfractures nearby them. Therefore, for efficient

hydraulic fracturing design, it is vital to determine the distribution of kerogen in shale and their mechanical properties.

Moreover, as discussed above, most of shale gas and oil are stored in the pores of organic components such as kerogen. For conventional reservoirs, permeability is unrelated to the pore well materials because of the larger pore sizes and small portion of hydrocarbons on the pore surface. However, in shale and kerogen, the large portion of pores is as small as several to tens of nanometers. The transportation of hydrocarbon molecules is greatly affected by adsorption/desorption and other interactions between these molecules and pore well. For a reservoir engineer, to accurately describe the recovery of shale gas and oil from hydraulic fractured horizontal well, it is pivotal to theoretically understand these interactions and develop the methods to quantify them.

For conventional reservoirs, the fluid transportation is described by continuum mechanics developed based on the continuum assumption. However, at the level of nanometers, the continuum assumption is not valid anymore. At this level of resolution, the molecule structures of both fluid and pore wall can be distinguished and thus other methods such as molecular dynamics simulation have to be used to describe and understand the adsorption, collision and transportation of fluid molecules in these nanochannels. While the fluid molecule structure models are well developed, the key problem of such calculation now is the lack of a reasonable 3D structure model of kerogen. With such a model, all the mechanisms for the storage, adsorption and migration of hydrocarbons in the nanopores of shale can be explored and clarified theoretically as the basis for the shale reservoir simulation and EOR. Therefore, 3D

kerogen molecule structure modeling is also the key for accurate shale reservoir simulation and EOR.

3.6 Previous work on kerogen modeling

As discussed above, kerogen structure modeling is currently of great importance for petroleum industry. There are two levels of kerogen structure modeling: 2D and 3D. To calculate the various physical and chemical properties of kerogen, a 3D structure is the final goal of kerogen modeling. However, a 2D molecule structure is the indispensable basis to build the 3D model. In the following sections, both the 2D and 3D kerogen modeling will be reviewed.

3.6.1. 2D molecular model of kerogen

Up to now, only a few 2D kerogen molecule structures have been proposed based on chemical and instrumental analysis. In 1969, Burlingame et al.[2] studied the kerogen of the Green River formation with gas liquid chromatography and mass spectroscopy (MS) using chromic acid in sulfuric acid. Later on, in 1971, Djuricic et al.[3] used permanganate oxidation method to study the Green River kerogen. In 1974, Schmidt-Collerus and Prien[4] investigated the structure of Green River oil shale by a combination of micropyrolysis and MS. In 1974, Yen[5] further studied the Green River oil shale kerogen based on X-ray diffraction and elemental analysis. As the initial work in this area, instead of a complete 2D structure of kerogen, only the information of the 2D structures of some possible kerogen fragments and possible ways of organizing these fragments were proposed in these papers.

It was until 1980[6] that Durand and co-workers proposed several complete 2D molecular structures of type I and type II kerogens in their book: *Kerogen, Insoluble Organic Matter from Rocks*.

In 1987, Behar et al.[7] proposed several 2D molecular structures for type I, II and III kerogens at the beginning of diagenesis and the end of catagenesis combining the analytical data of elemental analysis, electron microscopy, ^{13}C NMR, thermogravimetry, functional analysis and pyrolysis.

In 1995, Siskin et al.[8] proposed a 2D model for type I Green River oil shale and a 2D kerogen model for Rundle Ramsay Crossing oil shale. The two models were proposed based on nondestructive chemical derivatization and characterization of Green River oil shale materials isolated under mild conditions via NMR and MS analysis.

In 2003, Lille et al.[9] also proposed a 2D model for Estonian kukersite kerogen, a type II/I kerogen based on ^{13}C MAS NMR spectrum study.

In 2004, Siskin et al.[10] revisited their Green River oil shale model and compared to the results from further characterization of Green River oil shale by NMR, XPS (X-ray photoemission spectroscopy) and sulfur XANES (X-ray absorption near edge structure).

In 2006, a more general 2D Green River oil shale kerogen model with approximately one million atoms was developed by Siskin et al.[11] using the results from various solid state analysis. The model was further applied to predict oil and gas compositional yields from kerogen thermal decomposition reaction. However, this model is too large for property calculation using current computational chemistry techniques.

3.6.2 3D kerogen modeling

In a book published in 1976, a picture of 3D structure model of Green River oil shale was shown[12]. However, neither the method to construct this model nor the structure information in details was discussed.

Faulon Model

In 1989, the first 3D kerogen macromolecular model was created by Faulon et al.[13] using an in-house software: Xmol™ programmed specifically to build this 3D model on APOLLO stations. The 3D structure of a type III kerogen was shown as an example. From this model, the mircroporosity of kerogen was directly visualized. It was a pity that no quantitative physical properties were calculated based on this model. One important point of view proposed in this paper is as following: “analytical techniques on a mixture of various macromolecules, such as kerogen, give also data which are averaged in comparison with the real chemical structure, thus a perfect knowledge of this real structure has no meaning. The modeling of such macromolecules by an average structure is thus a necessity.” The meaning of this conclusion will be discussed in details later.

Orendt Model

With the surge of the recovery of shale reservoirs, the structure and properties of kerogen attract much more attention than before. In 2012, Orendt et al.[14] proposed a method to construct a 3D structural model of the Green River oil shale using a combination of ab initio and molecular mechanics calculations based on the 2D Siskin’s

Green River oil shale kerogen model. The initial 3D structure was built using the software of HyperChem via the molecular mechanics energy minimization method based on the MM+ force field. The structure was further optimized with the quantum chemical ab initio method using the software package of GAMESS at the restricted Hartree-Forck (RHF) level of theory based on the minimal STO-3G basis set. Using this structure as the starting model, four 3D models of kerogen were acquired by the molecular mechanics calculations using simulated annealing method. There were three steps in this algorithm: heat (from 10K to 1200K at a rate of 119K/0.01ps), run (at 1200K for 0.5ps), and cool (from 1200K to 300K at a rate of 9K/0.01ps). By this method, different configurations can be obtained from the same initial 3D structure randomly. From these four configurations, the structure with the lowest overall energy was selected as the "parent" for the next simulated annealing circle, from which five new configurations were obtained. Among these five 3D structures, the one with the lowest overall energy was selected as the final 3D model of kerogen that was further applied for property calculation of kerogen, such as ^{13}C NMR and pair distribution function (PDF). The calculation results showed reasonably good agreement with experimental results. This represents a significant progress in kerogen modeling study because theoretical results were compared with experiments results to evaluate the proposed model.

3.7 Limitations of previous work

Due to the importance of kerogen in oil/gas generation mechanism, oil shale and shale oil/gas recovery, elucidation of 3D kerogen structure has attracted great attention in petroleum industry and academy. Previously, based on a series of characterization

techniques, such as GC-MS, LC-MS, NMR and pyrolysis GC, several 2D kerogen molecular structures have been proposed. With these 2D models as a reasonable starting point, some 3D kerogen models have been constructed which represents significant progresses in kerogen study. However, there are some drawbacks with these models that limit their practical applications:

1. Kerogen is essentially a mixture of multiple molecules, while in these models only the 3D structure of one molecule was modeled. The problem about how to combine and assemble multiple molecules into one kerogen model was essentially avoided in these reports. However, to build a realistic kerogen 3D model, methods have to be developed to assemble multiple molecules together in a reasonable scientific way;

2. In reality, kerogen is a kind of insoluble solid material while the 3D kerogen models in previous reports are essentially the models of macromolecules. In fact, the macromolecules in the sizes of these reports are soluble in water or organic solvents. For example, proteins and DNA in these sizes in our cells are soluble in water. Therefore, instead of the macromolecule model, a suitable way must be figured out to build a solid state model of kerogen based on the 2D structures developed previously.

3. These previous models are in fact built in vacuum without the parameters of pressure. As a result, some important mechanical properties, such as Young's modules and Poisson ratios cannot be calculated using these models although they are of great importance to hydraulic fracturing design.

Chapter 3: Theory

3.1 Quantum chemistry calculation

Our world is made of various materials. Materials are made of molecules and atoms. Atoms are made of nucleus and electrons. The diameter of the nucleus is in the range of 1.75 fm (hydrogen) to about 15 fm (uranium) that is much smaller than the diameter of the atom itself, by a factor of about 145,000 (hydrogen) and about 23,000 (uranium). Most volume of the atoms is occupied by the electrons which move around the nucleus at nearly light speed. According to modern physics and computational chemistry, all the properties of materials are determined by the electron configuration of the materials.

The theory that describes the motion and interaction of subatomic particles is quantum mechanics. The fundamental equation of quantum mechanics is Schrödinger equation:

$$\left[\frac{-\hbar^2}{2m}\nabla^2 + V\right]\psi = i\hbar\frac{\partial}{\partial t}\psi$$

$$\nabla^2 = \frac{\partial^2}{\partial^2 x} + \frac{\partial^2}{\partial^2 y} + \frac{\partial^2}{\partial^2 z}$$

$$\hbar = \frac{h}{2\pi}$$

For a one-electron atom, hydrogen which is the simplest atom system, the potential energy term can be given by Coulomb's law:

$$V = -\frac{Ze^2}{4\pi\varepsilon_o r}$$

The total energy operator $\hat{H}$ is

$$\hat{H} = -\frac{h^2}{8M\pi^2}\nabla_N^2 - \frac{h^2}{8m\pi^2}\nabla^2 - \frac{Ze^2}{4\pi\varepsilon_o r}$$

The first term in the right hand represents the kinetic energy of nucleus; the second term is the kinetic energy term of electron and the third one is the potential term. According to the Born–Oppenheimer (BO) approximation, which assumes the motion of atomic nuclei and electrons in a molecule can be separated, $\hat{H}$ can be simplified as:

$$\hat{H} = -\frac{h^2}{8m\pi^2}\nabla^2 - \frac{Ze^2}{4\pi\varepsilon_o r}$$

The solution of this equation is well established:

$$\Psi_{nlm} = R_{nl}(r)Y_{lm}(\theta,\phi)$$

n is the principal quantum number (0, 1, 2, …); l is the azimuthal quantum number (0, 1, …(n-1)) and m is the magnetic quantum number (-l, -(l-1),…0…(l-1), l).

$$R_{nl}(r) = -[(\frac{2Z}{na_o})^3 \frac{(n-l-1)!}{2n[(n+l)!]^3}]^{1/2}\exp(-\frac{\rho}{2})\rho^l L_{n+1}^{2l+1}(\rho)$$

a_o is the Bohr radius. $L_{n+1}^{2l+1}(\rho)$is a Laguerre polynomial.

$$Y_{lm}(\theta,\phi) = \Theta_{lm}(\theta)\Phi_m(\phi)$$

$$\Theta_{lm}(\theta) = \frac{1}{\sqrt{2\pi}}\exp(im\phi)$$

$$\Phi_m(\phi)=[\frac{(2l+1)}{2}\frac{(l-|m|!)!}{(l+|m|!}]^{1/2}P_l^{|m|}(\cos\theta)$$

$P_l^{|m|}(\cos\theta)$ is the associated Legendre polynomials.

Some solutions of the Schrödinger equation of hydrogen are illustrated in Fig. 3.1[15].

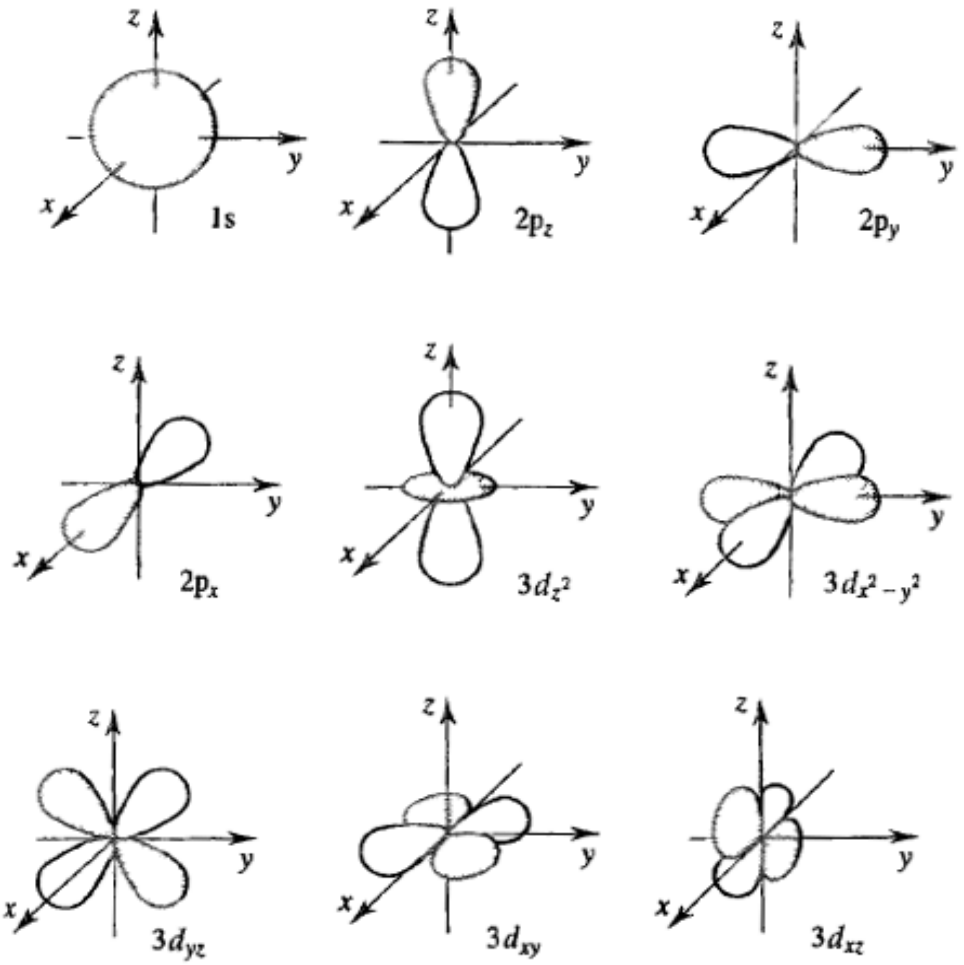

Figure 3.1 The common graphical representations of s (n=1, l=0), p (n=2, p=1, 0, -1) and d (n=3, l=2, 1, 0, -1, -2) orbitals of hydrogen.

For polyelectronic atomic systems, exact solutions are not achievable, but many different approximation methods were developed to handle this problem.

Different atoms can combined together to form various molecules. The electronic configuration of molecules can be obtained by a linear combination of atomic orbitals (LCAO approach).

$$\boldsymbol{\psi_i} = \sum_{\boldsymbol{\mu=1}}^{\boldsymbol{K}} \boldsymbol{c_{\mu i}\phi_{\mu i}}$$

$\boldsymbol{\psi_i}$ represents a molecular orbital, $\boldsymbol{c_{\mu i}}$ represents a coefficient and $\boldsymbol{\phi_{\mu i}}$ represents one of K atomic orbitals. Besides the analytical solutions, Gaussian functions from standard basis sets are also often applied as orbital functions.

Based on the variation theorem, the coefficient can be determined by the following equations:

$$\frac{\boldsymbol{\partial \bar{E}}}{\boldsymbol{\partial c_1}} = \frac{\boldsymbol{\partial \bar{E}}}{\boldsymbol{\partial c_2}} = \cdots = \frac{\boldsymbol{\partial \bar{E}}}{\boldsymbol{\partial c_n}} = \cdots \equiv \mathbf{0}$$

Once the coefficients are determined, the molecular orbitals are determined and all the properties of the materials can be calculated theoretically.

3.2 Molecular Dynamics Simulation

In principle, all the properties of materials should be calculated by quantum chemistry methods. However, this type of calculation is very time-consuming which severely limited their application in large systems. To calculate systems with significant amounts of atoms, some simpler approximate methods must be developed to achieve results accurate enough in acceptable tolerance but much more efficiently. Molecular dynamics simulation is one of such methods[15].

The key simplification of molecular dynamics simulation is to use the empirical potential functions to describe the interaction between atoms instead of complicated quantum calculation. These empirical potentials, or normally termed as force fields, are derived from experimental results or quantum chemistry calculations. These empirical potentials consist of a summation of bonded forces and non-bonded forces such as van der Waals forces and electrostatic charge.

$$U_{total}=U_{NB}+U_{B}$$

$$U_{NB}=U_{VW}+U_{E}$$

$$U_{B}=U_{bond}+U_{angle}+U_{dihedral}$$

U_{total} is the total energy of a system, U_{NB} is the non-bonded energy, U_B is bonded energy, U_{VW} is the energy related to van der Waals interaction and U_E is the energy related to electrostatic interaction, U_{bond} is the bonding energy, U_{angle} is bond angle bending energy and $U_{dihedral}$ is the dihedral angle potential energy respectively.

Electrostatic interaction can be determined by Coulomb' law:

$$U_E=\frac{q_1 q_2}{4\pi\varepsilon_o r}$$

The van der Waals interaction is normally described by 12-6 Lennard-Jones potential:

$$U_{VW}=4\varepsilon[(\frac{\sigma}{r})^{12}-(\frac{\sigma}{r})^{6}]$$

U_{bond} is controlled by Hook's law:

$$U_{bond}=\frac{1}{2}\boldsymbol{k}(\boldsymbol{r}-\boldsymbol{r_o})^2$$

U_{angle} and $U_{dihedral}$ are modeled as following:

$$U_{angle}=\frac{1}{2}\boldsymbol{k_\theta}(\boldsymbol{\theta}-\boldsymbol{\theta_o})^2$$

$$U_{dihedral}=c_0 + c_1[1+\cos(\phi)] + c_2[1-\cos(2\phi)] + c_3[1+\cos(3\phi)]$$

With these models, the inter- and intra-molecule interaction in static states can be calculated in an efficient way which allows the theoretical calculation of large systems.

Furthermore, the kinetics properties of these systems and atomic movement can be calculated based on Newton's equation of motion. After determination of interaction forces between the atoms from the gradient of potentials, the movement and trajectory of the atoms can be tracing by solving Newton's equations based on the following equations:

$$F_i = -\frac{\partial U_i}{\partial r_i}$$

$$F_i = m_i \frac{d^2 r_i}{dt^2} = m_i a_i$$

By this method, molecular dynamics simulation provides a way to handle many-body problem (1,000-100,000 atoms). For such a system, the possible states can be classified according to statistical ensemble. Two types of ensembles used in this thesis are the canonical (NVT) ensemble and the isothermal-isobaric (NPT) ensemble. N is the number of molecules, V is the volume, P is the pressure and T is the temperature. Canonical or constant-temperature, constant-volume ensemble (NVT) describes a

system with constant temperature, volume and the number of molecules in contact with a heat bath. The temperature of the ensemble is controlled by direct temperature scaling at the initialization stage and through temperature-bath coupling at the data collection phase. Isothermal-isobaric (NPT) ensemble allows control of both pressure and temperature. The pressure is controlled by adjusting the volume. This ensemble can be used to achieve the desired temperature and pressure.

Chapter 4: 3D Kerogen Modeling and its Mechanical/Spectral Property Calculation

4.1 Establishment of the 3D model of kerogen

In this chapter, the method to construct a 3D model of Green River oil shale kerogen will be proposed. There are mainly four steps to build this model:

1. Select a suitable 2D model as the basis to build the 3D model;

2. Build the 3D model of the seven individual molecules as the build units of kerogen. As mention previously, most of current kerogen models are built based on one macromolecule. However, real kerogen is always a mixture of many different molecules. Different from previous work, in this thesis a method to build a model of kerogen as a mixture is proposed. As the basis of this work, the 3D models of seven molecules as the building units of kerogen were first built;

3. The next step to build the model, a method to build a molecular nanocluster model is proposed. Obviously, with the 3D models of the building units available, the next step is how to assemble them. In this step, we proposed to assemble these molecules by an adsorption method. It was found that different adsorption sequences will induce different molecular nanoclusters and different adsorption energy released totally. Based on different adsorption sequences, 24 molecular nanocluster models of kerogen were obtained. The one releasing the most adsorption energy was selected for the final step to build a solid state model of kerogen;

4. In the final step, based on the MD simulation method, we build a solid state model of kerogen. As mentioned before, most of previous kerogen models are only macromolecule models built under vacuum since there are no parameters related to pressure endowed to these models. Here, based on the MD simulation method, the parameter of pressure is endowed to the kerogen model. Therefore, our model of kerogen is a real solid state model.

In addition, it should be mentioned that COMPASS force field is selected in this thesis to build the 3D molecule models as the building unit of kerogen, molecular nanocluster model of kerogen and solid state model kerogen. This is because the COMPASS force field has successfully been applied to predict the mechanical properties of organic-inorganic hybrid material[16]. Hydraulic fracturing plays a key role in the recovery of shale reservoirs. Mechanical properties of shales are the most important parameters for hydraulic fracturing design. One of the most important applications of the proposed model is to calculate the mechanical properties of shale for the purpose of better hydraulic fracturing design. Shale is a mixture of organic materials such as kerogen and inorganic materials such as quartz and clays. As the first step to calculate the mechanical properties of shale, the organic component of shale: kerogen is modeled in this thesis. In future, the proposed model may be further applied to be combined with inorganic materials to build a shale model. This model will be a hybrid of organic and inorganic materials. Since the mechanical properties of such a system have been successfully predicted by the COMPASS force field, as the basis for future work, the COMPASS force field was selected to build the kerogen model.

4.1.1 Selection of a 2D model

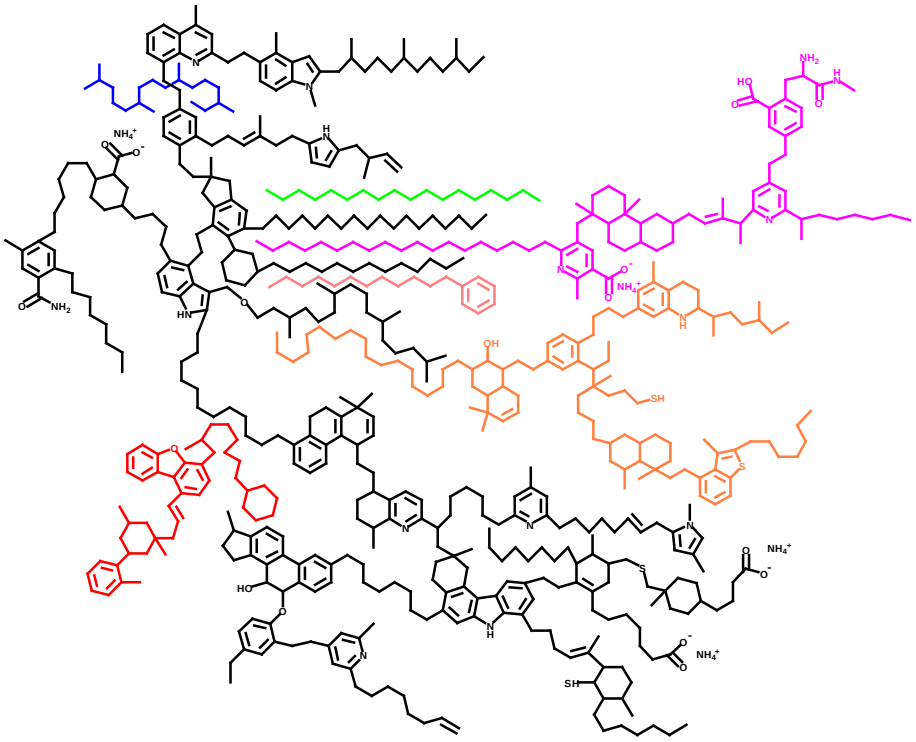

Figure 4.1 The 2D molecular structure of Green River oil shale kerogen proposed by Siskin et al. There are seven molecules in the 2D molecular structure: 1 (black), 2 (orange), 3 (magenta) 4 (red), 5 (blue), 6 (light coral) and 7 (green).

In this thesis, the 2D kerogen model of Green River oil shale proposed by Siskin et al.[8] in 1995 is chosen as the basis to build the 3D model of kerogen mainly for the following reasons:

1. As mentioned earlier, to justify the proposed 3D kerogen model, the physical/chemical properties of kerogen have to be calculated theoretically based on the model and compared with experimental results. Although several 2D structures of kerogen from different plays have been proposed, few experimental data are available

about their physical/chemical properties. Fortunately, many experimental data of such kind are available for the Green River oil shale kerogen;

2. There are about 1900 atoms in this model that is large enough to represent a typical unit of kerogen and small enough to match the calculation capability of current computational chemistry;

3. Green River formation is the largest oil shale deposits in the world, the estimated oil resource in place of which ranges from 1.2 to 1.8 trillion barrels. It is one of the most promising deposits for commercial applications. Some projects have been started by oil companies, such as Chevron, Shell, IDT and OSEC to explore the possibility of extracting oil from oil shale in this area.

Therefore, Siskin Green River Oil Shale kerogen 2D model shown in Fig. 4.1 is selected as the basis to build a 3D kerogen model.

4.1.2 The 3D Models of Seven Molecules as the Building Unit of Kerogen

The 2D molecular structure of Green River oil shale kerogen proposed by Siskin et al.[8] is shown in Fig. 4.1. This kerogen is composed of seven molecules. To build the kerogen model, first the 3D models of the seven individual molecules were built and the structures were improved by geometry optimization using COMPASS force field in the Forcite module of Material Studio 7.0. The configurations of the seven molecules were further optimized by a simulated annealing method in the Forcite module, during which the temperature increased from an initial temperature (298K) to a midcycle temperature (1200K) and decreased back to the initial temperature periodically. The process was

performed for 10 cycles using the COMPASS force field. The purpose of this process is to identify the different local minimum energy configurations using the higher temperature periods of each cycle to overcome energy barriers and the configuration with the lowest energy was applied to the subsequent adsorption calculation. The obtained structures of molecules 1 to 7 after annealing are shown in Fig. 4.2 to 4.8.

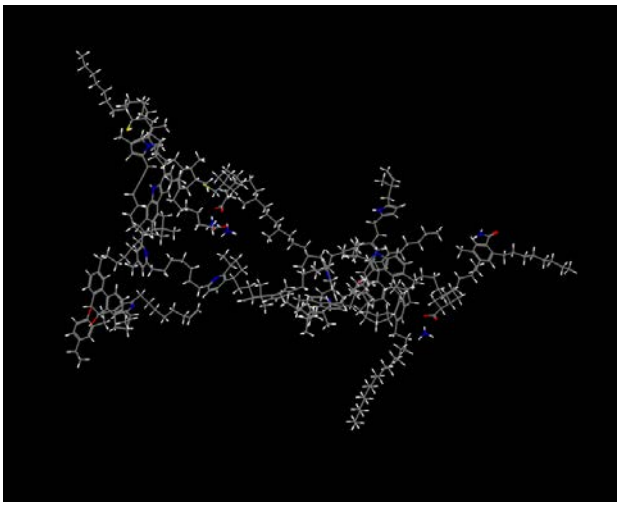

Figure 4.2 Illustration of the optimized 3D structure of the molecule 1 in the Siskin's Green River oil shale kerogen model.

Figure 4.3 Illustration of the optimized 3D structure of the molecule 2 in the Siskin's Green River oil shale kerogen model.

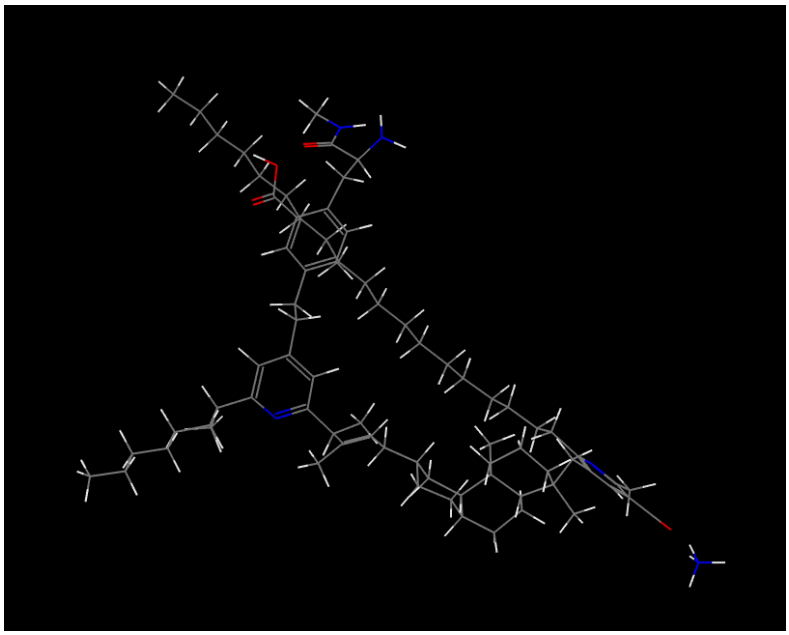

Figure 4.4 Illustration of the optimized 3D structure of the molecule 3 in the Siskin's Green River oil shale kerogen model.

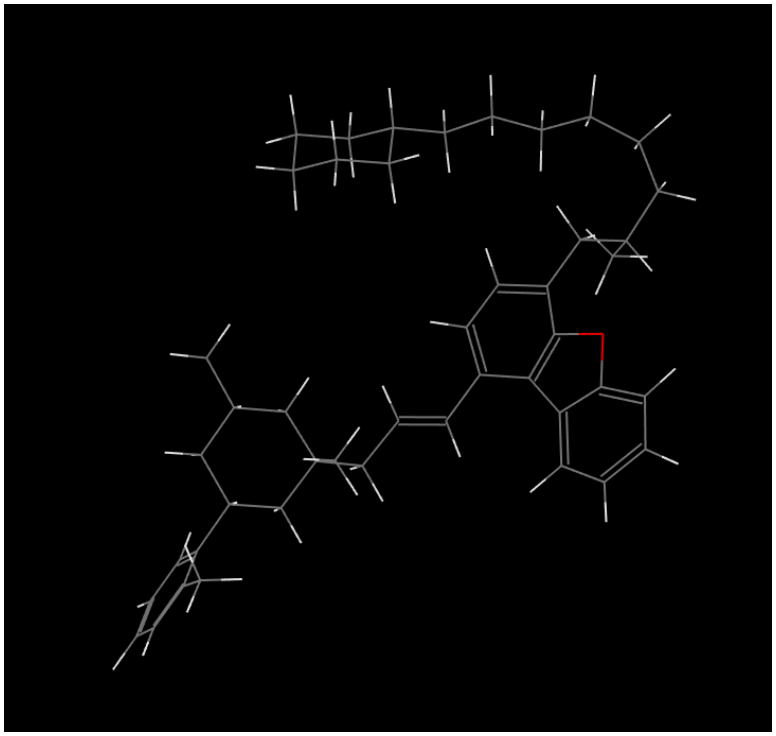

Figure 4.5 Illustration of the optimized 3D structure of the molecule 4 in the Siskin's Green River oil shale kerogen model.

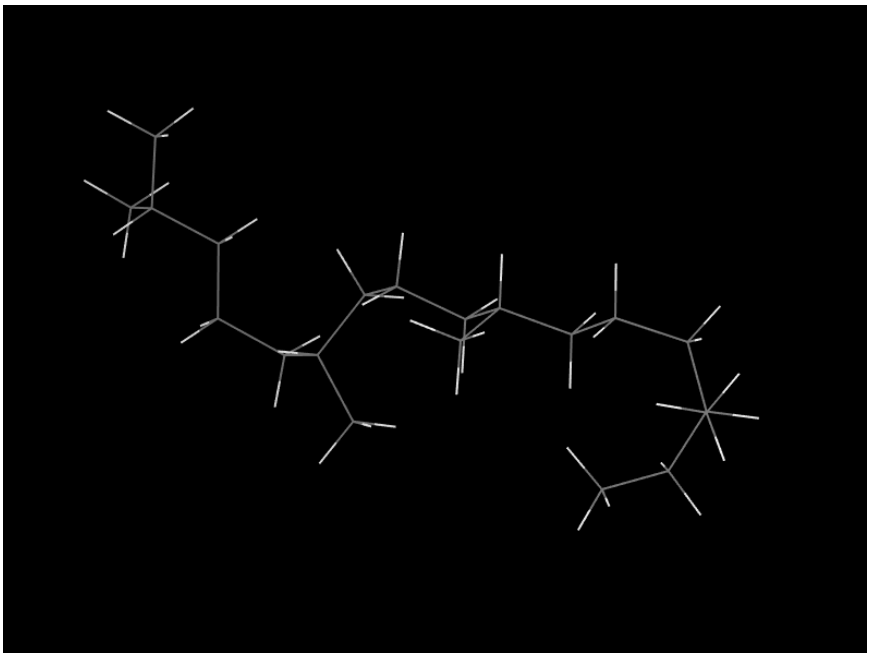

Figure 4.6 Illustration of the optimized 3D structure of the molecule 5 in the Siskin's Green River oil shale kerogen model.

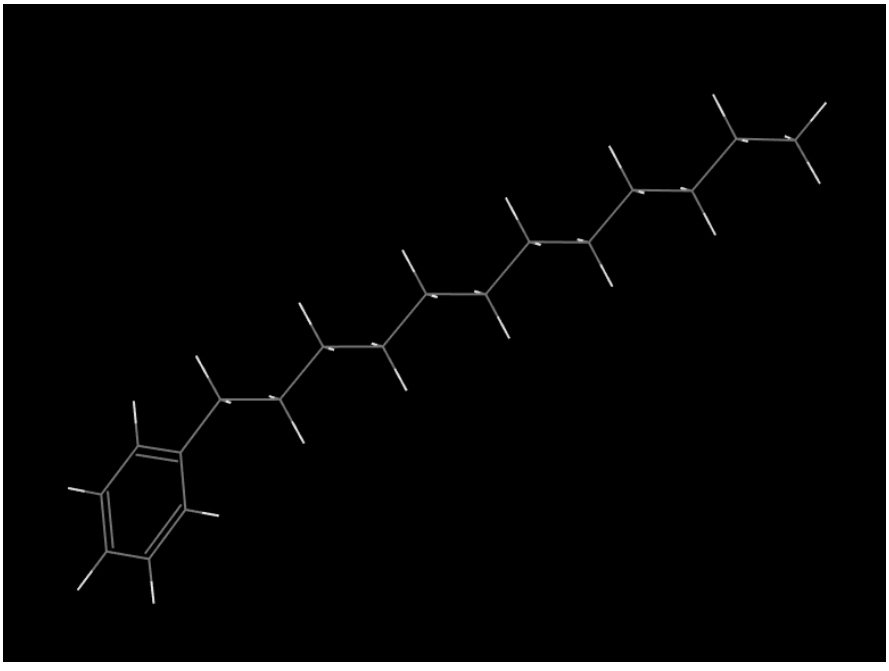

Figure 4.7 Illustration of the optimized 3D structure of the molecule 6 in the Siskin's Green River oil shale kerogen model.

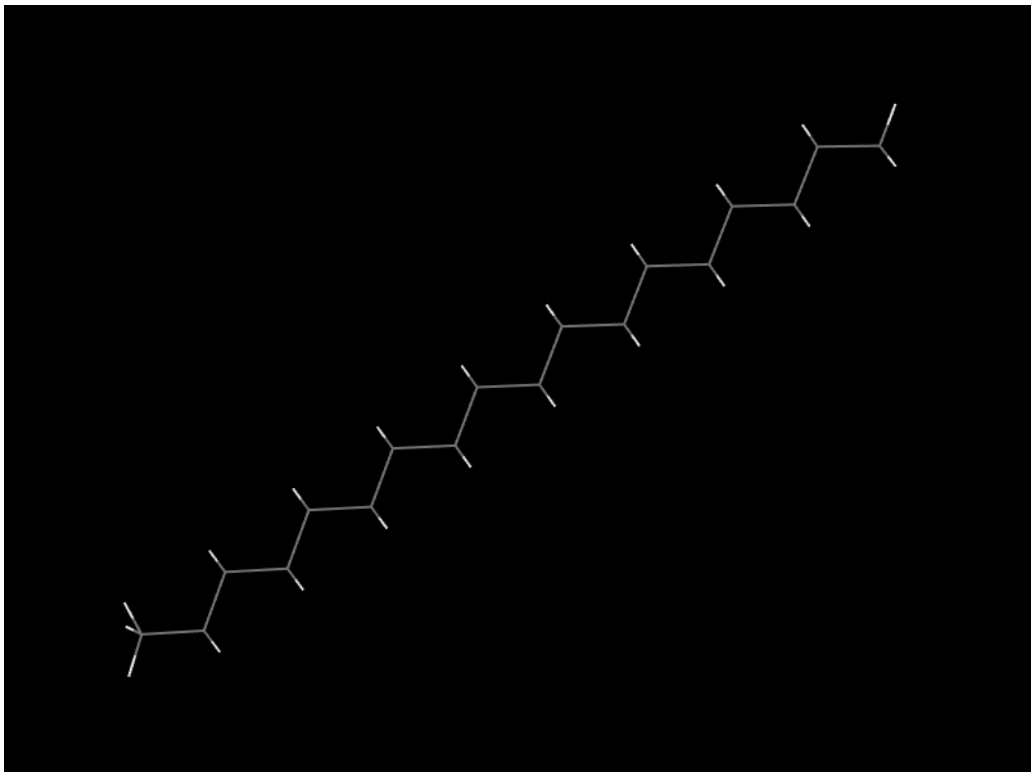

Figure 4.8 Illustration of the optimized 3D structure of the molecule 7 in the Siskin's Green River oil shale kerogen model.

4.1.3 The Molecular Nanocluster Model of Kerogen

The seven molecules were further combined together to a molecular nanocluster using the Adsorption Locator module of Materials Studio 7.0. In principle, there are infinite combinations of the seven molecules spatially. In reality, the most thermodynamically stable system is the one with the lowest energy. The interaction of two molecules during the combination process can be viewed as an adsorption process. The more adsorption energy is released, the more stable the system is. Using the Adsorption Locator module of Materials Studio 7.0 which is based on the Monte Carlo method, the adsorption energy released during the combination of the molecules can be calculated. Our study

reveals that the total released adsorption energy is determined by the addition sequence of the molecules. The functional groups are heterogeneously distributed in the molecules and there are some “hot spots” on the molecules where more adsorption energy will be released during adsorption. Once the “hot spot” is occupied by one molecule, it is not available for other molecules. Which molecule will occupy the “hot spot” is determined by the adsorption sequence. Therefore, the total released adsorption energy is in fact determined by the adsorption sequence of the molecules.

One problem is for 7 molecules, there are totally 720 (7!) possible sequences which requires a heavy computational burden. Therefore, an algorithm must be developed to find out the sequence with the minimal energy efficiently. With a careful examination of the 7 molecules shown in Fig.4 to 10, we propose such a method based on the following concerns:

1. Molecule 1 ($C_{366}H_{559}O_{10}N_{13}S_2$) is the largest molecule that accounts for over half of the total atoms in the kerogen model. Therefore, it is reasonable to select molecule 1 as the matrix for adsorption and add the other 6 molecules to this matrix to identify the optimal sequence;

2. The adsorption energy of the kerogen model is mainly determined by the adsorption energy released from large molecules. There are 273 atoms in molecule 2 ($C_{102}H_{167}ONS_2$) and only 62 atoms in molecule 5. Obviously the adsorption of molecule 2 to the matrix will release much more energy than that of molecule 5. Therefore, it is rational to allow the larger molecule to occupy the “hot spot” first which means more atoms can find best positions and release

more adsorption energy;

3. Due to the similarity of molecules 5 to 7, it is reasonable to postulate that the adsorption energy of these three molecules is small and close to each other.

Based on these considerations, it was realized that the seven molecules could be divided into three groups. Molecule 1 is the only member of group I acting as matrix. Group II includes the molecules 2 ($C_{102}H_{167}ONS_2$), 3 ($C_{75}H_{121}O_5N_5$) and 4 ($C_{45}H_{60}O$). Compared with group III, these molecules are larger and quite different from each other. Group III includes molecules 5 ($C_{20}H_{42}$), 6 ($C_{18}H_{30}$) and 7 ($C_{18}H_{38}$). These three small molecules have similar sizes and compositions. According to the above analysis, a two-step procedure is proposed to find out the kerogen model with the lowest energy. Since the adsorption energy of the kerogen model will be mainly dominated by the adsorption sequence of group II molecules, the first step should be the examination of the adsorption of group II molecules onto the matrix. There are only three molecules in this group. Therefore, there are totally 6 (3!) possible sequences, among which the sequence releasing the most energy can be identified. This sequence will be applied to the next step. In the second step, the absorption of group III molecules onto the model obtained from step I is examined. The sequence releasing most energy will be the one representing the kerogen nanocluster model. There are three molecules in group III and 6 possible sequences in the second step. For a full examination of the combination of all 7 molecules, 4320 (720×6) adsorption processes have to be calculated while with this two-step method, only 36 (6×3×2) adsorption processes need to be treated. The results of this method are shown in Fig. 4.9-4.14 and Table 4.1 and the 3D molecular structure

releasing the most energy(-962.58 Kcal/mol) with the sequence of 1243567 is shown in Fig. 4.9.

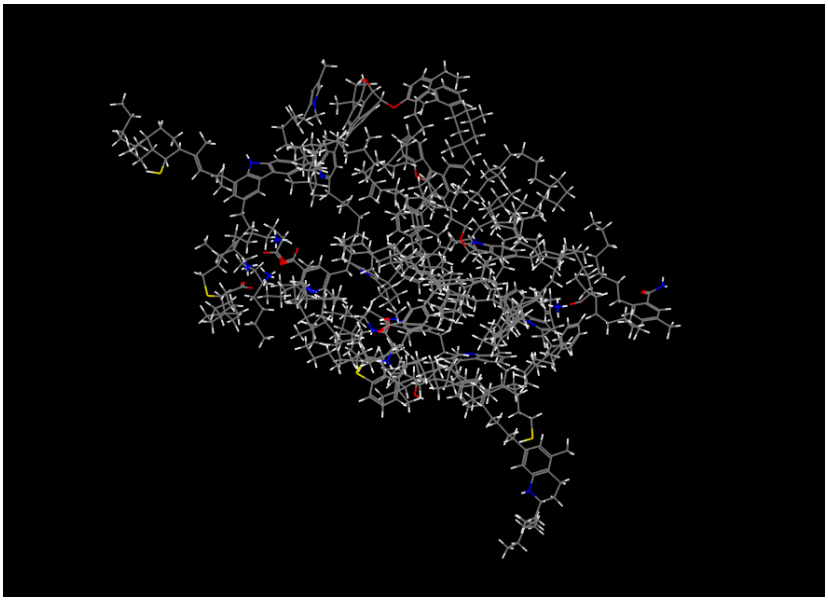

Figure 4.9 The 3D structures of kerogen nanoclusters formed by the adsorption sequence of 1243567.

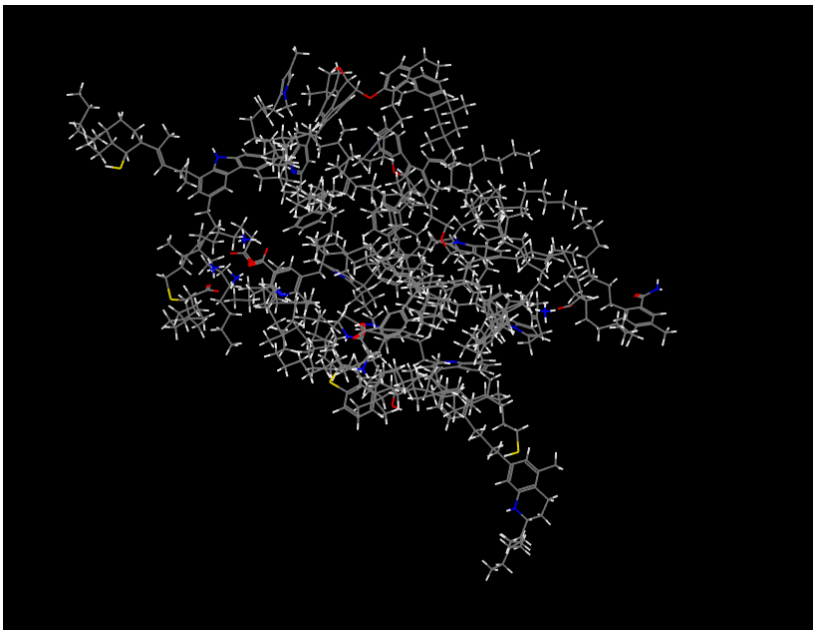

Figure 4.10 The 3D structures of kerogen nanoclusters formed by the adsorption sequence of 1243576.

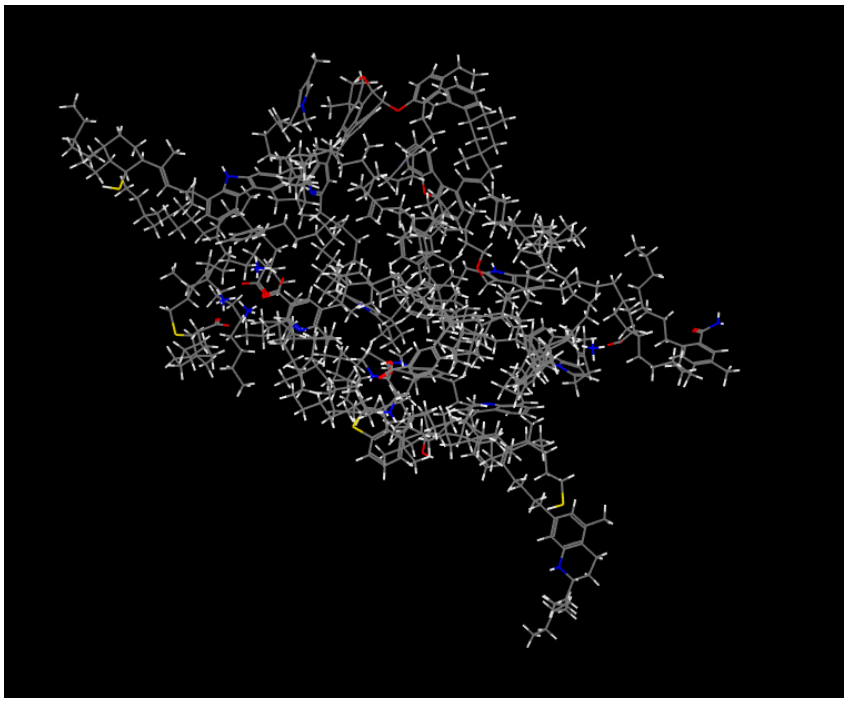

Figure 4.11 The 3D structures of kerogen nanoclusters formed by the adsorption sequence of 1243657.

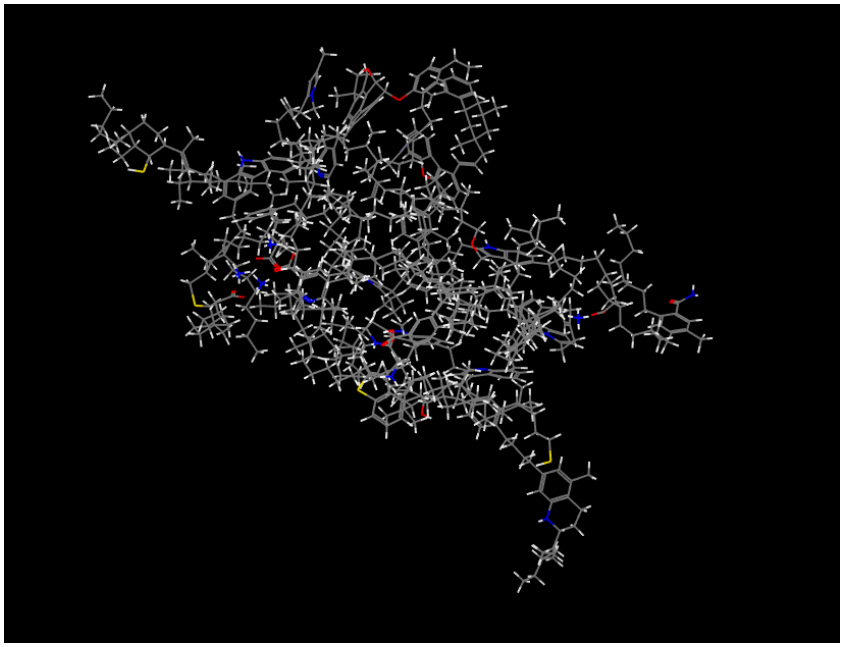

Figure 4.12 The 3D structures of kerogen nanoclusters formed by the adsorption sequence of 1243675.

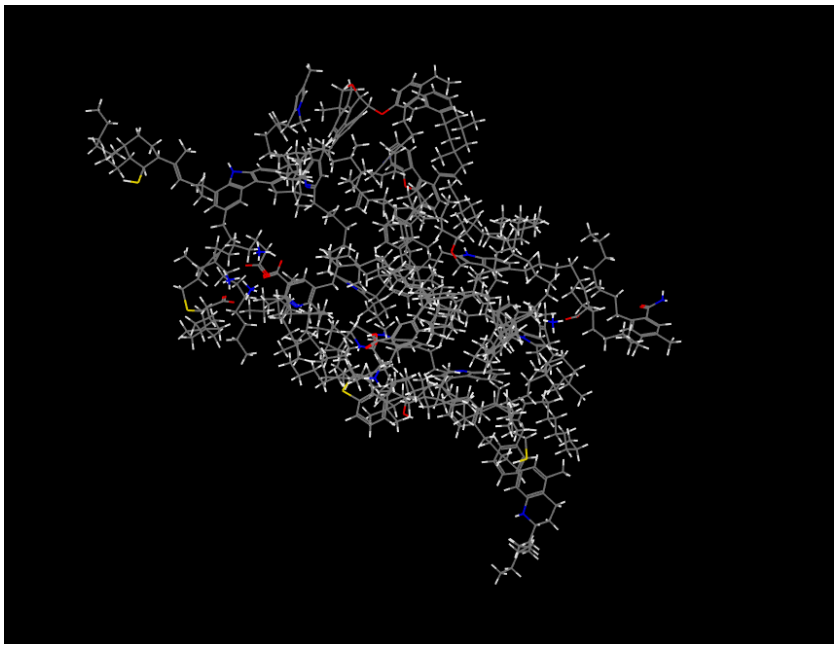

Figure 4.13 The 3D structures of kerogen nanoclusters formed by the adsorption sequence of 1243756.

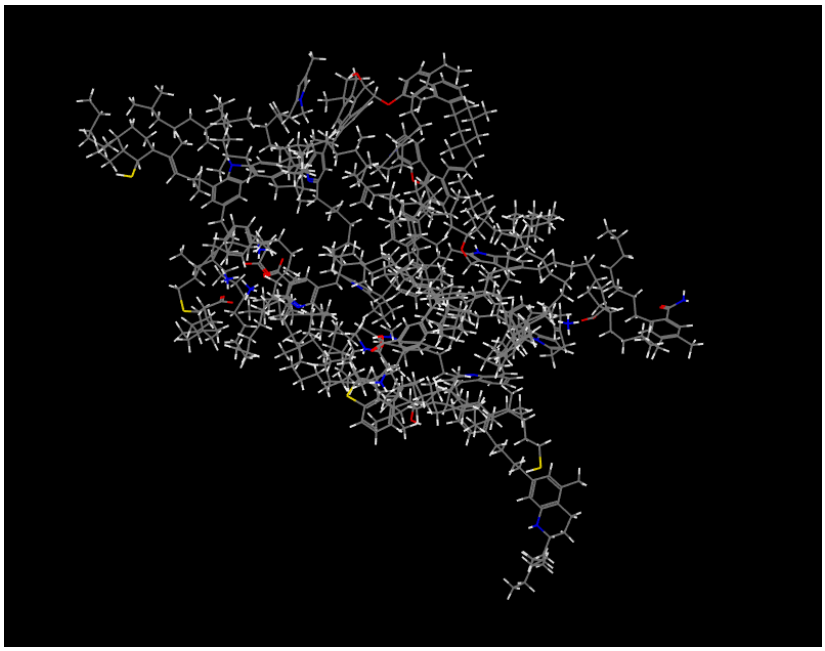

Figure 4.14 The 3D structures of kerogen nanoclusters formed by the adsorption sequence of 1243765.

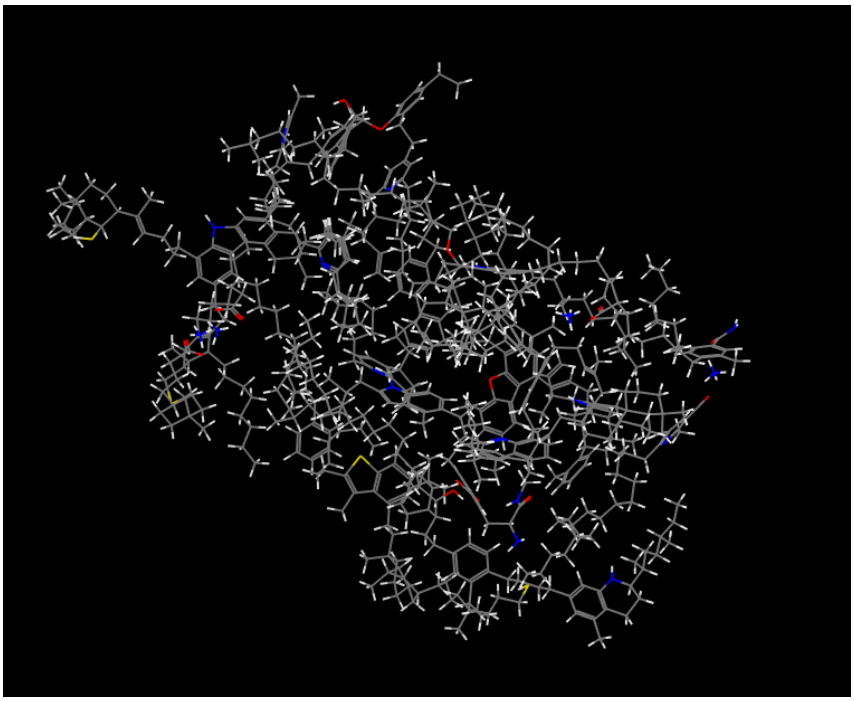

Figure 4.15 The 3D structures of kerogen nanoclusters formed by the adsorption sequence of 1324567.

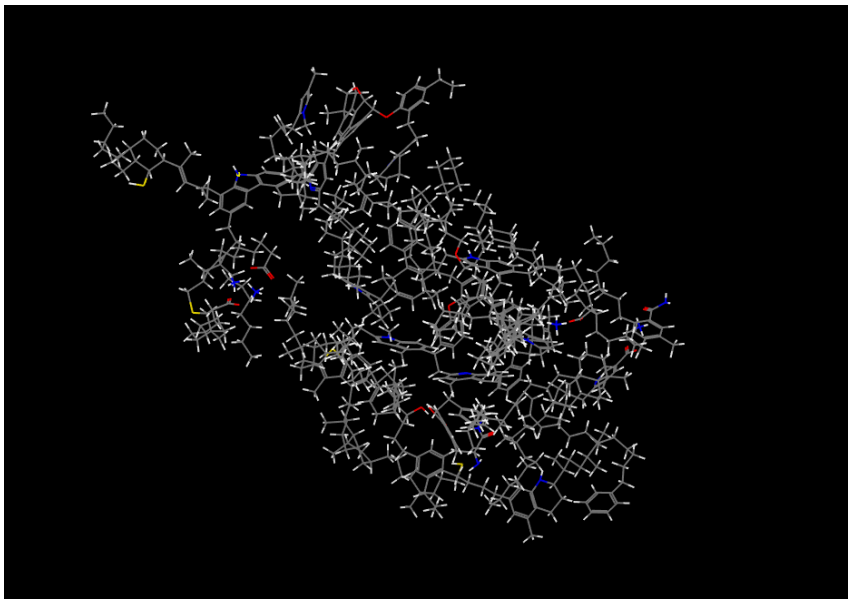

Figure 4.16 The 3D structures of kerogen nanoclusters formed by the adsorption sequence of 1324576.

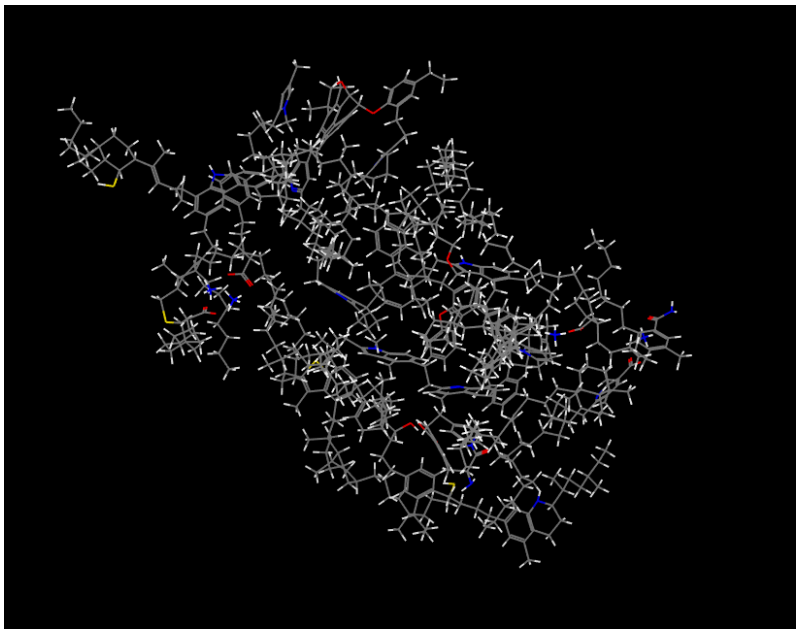

Figure 4.17 The 3D structures of kerogen nanoclusters formed by the adsorption sequence of 1324657.

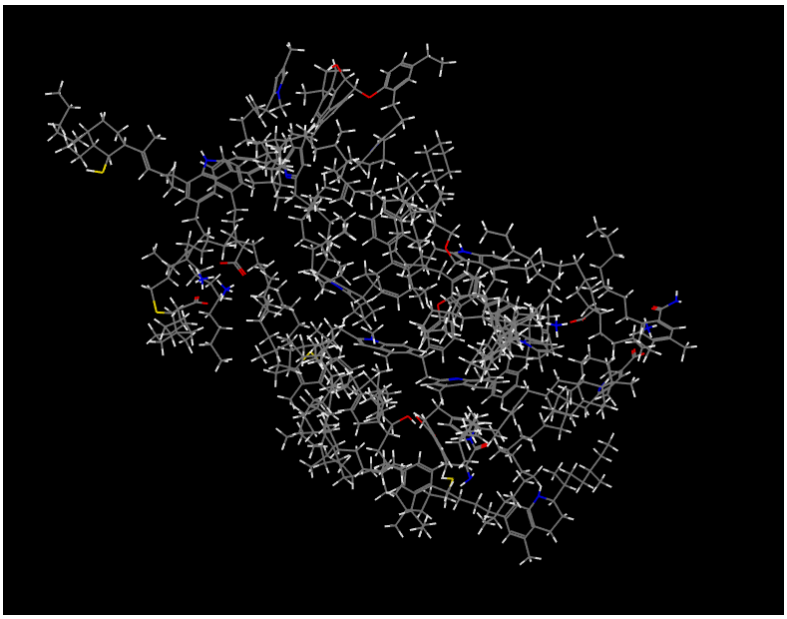

Figure 4.18 The 3D structures of kerogen nanoclusters formed by the adsorption sequence of 13246

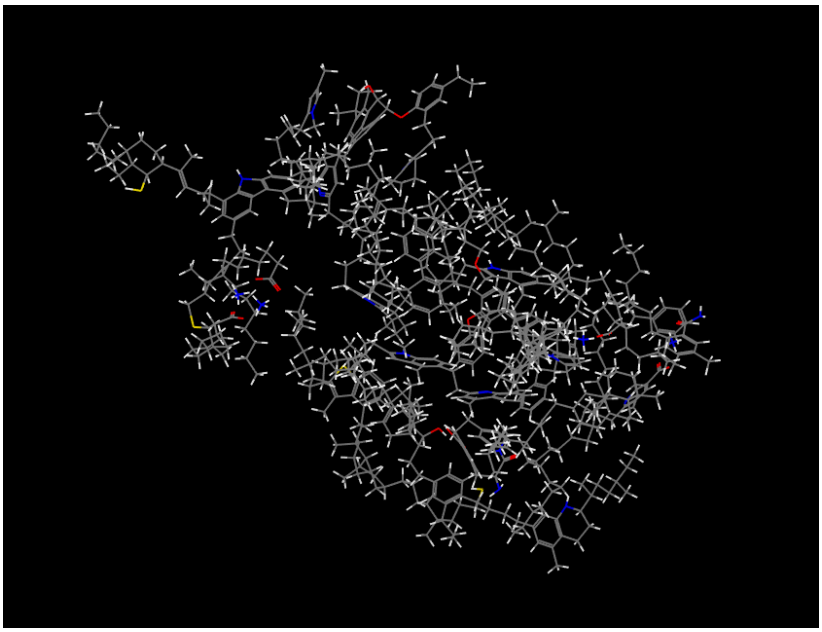

Figure 4.19 The 3D structures of kerogen nanoclusters formed by the adsorption sequence of 1324756.

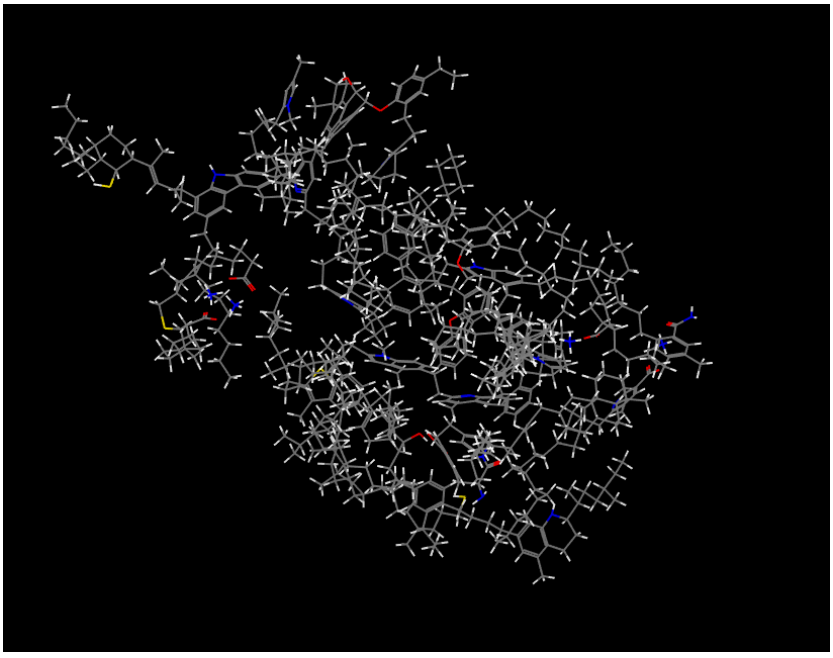

Fgure 4.20 The 3D structures of kerogen nanoclusters formed by the adsorption sequence of 1324765.

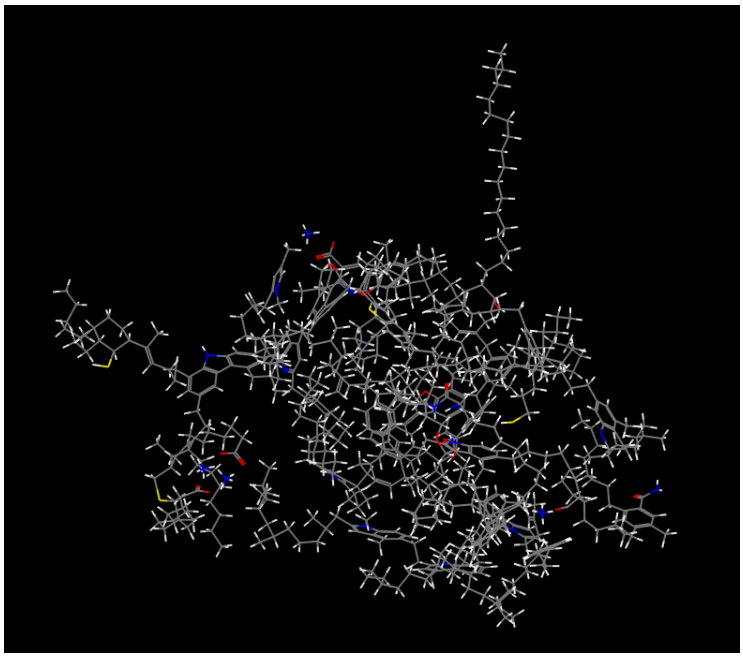

Figure 4.21 The 3D structures of kerogen nanoclusters formed by the adsorption sequence of 1657234.

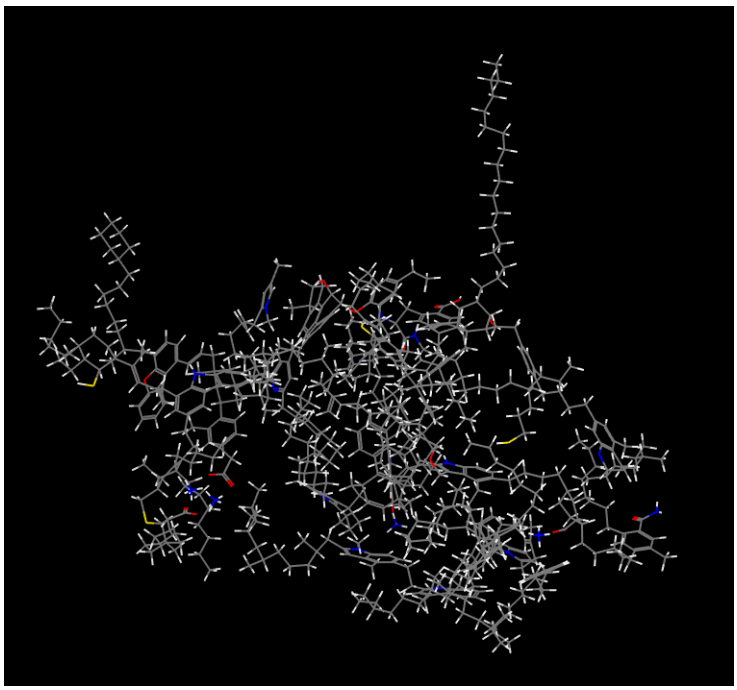

Figure 4.22 The 3D structures of kerogen nanoclusters formed by the adsorption sequence of 1657243.

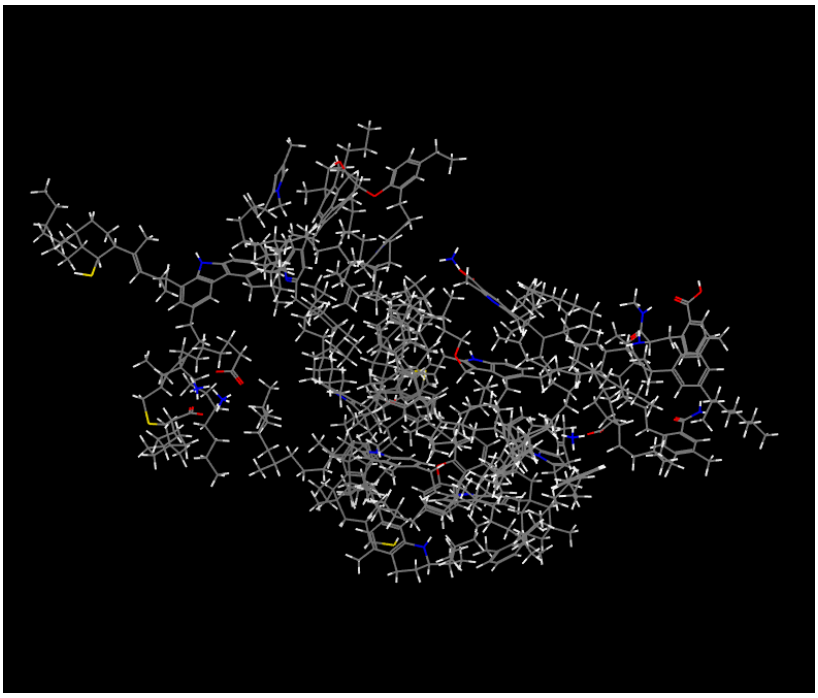

Figure 4.23 The 3D structures of kerogen nanoclusters formed by the adsorption sequence of 1657324.

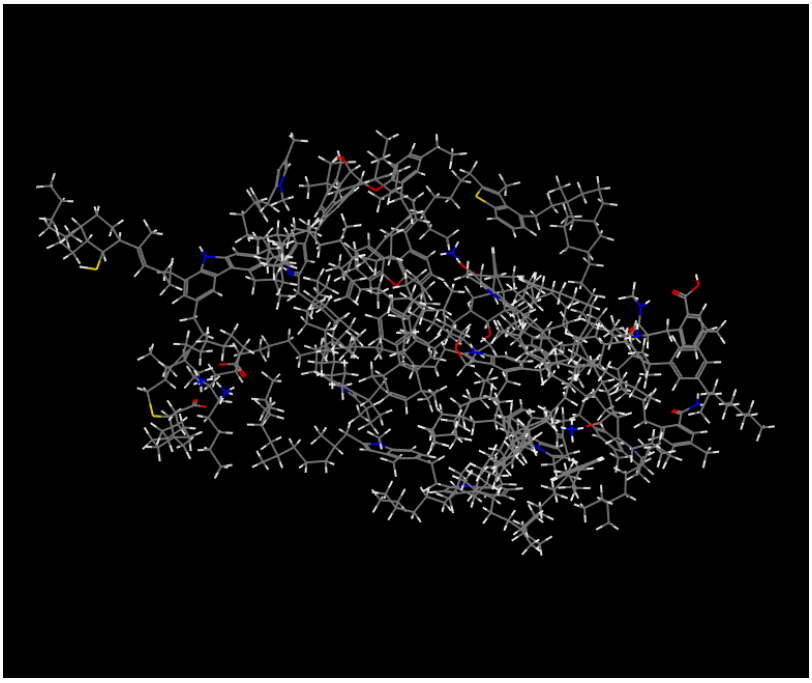

Figure 4.24 The 3D structures of kerogen nanoclusters formed by the adsorption sequence of 1657342.

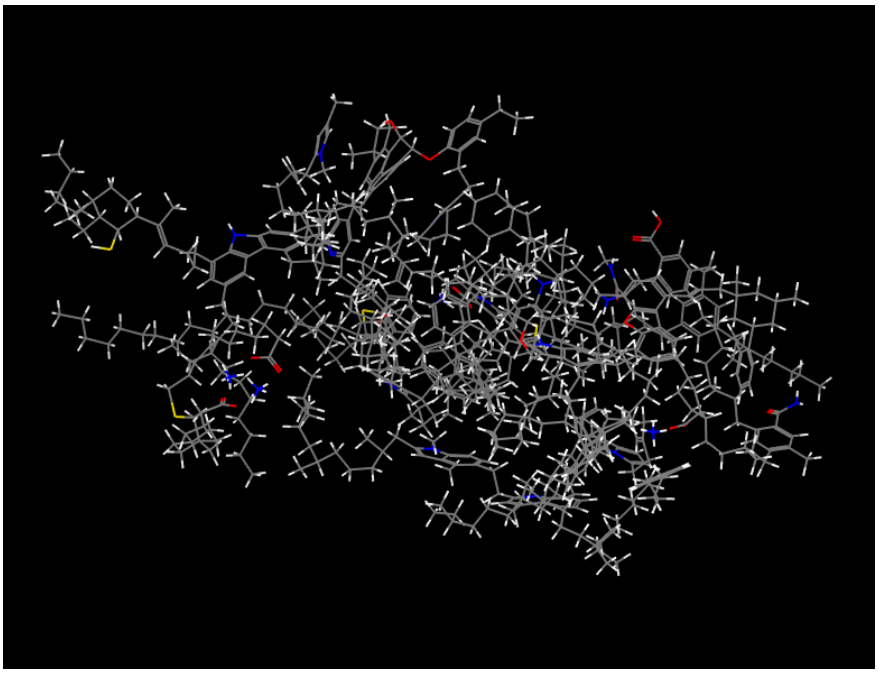

Figure 4.25 The 3D structures of kerogen nanoclusters formed by the adsorption sequence of 1657423.

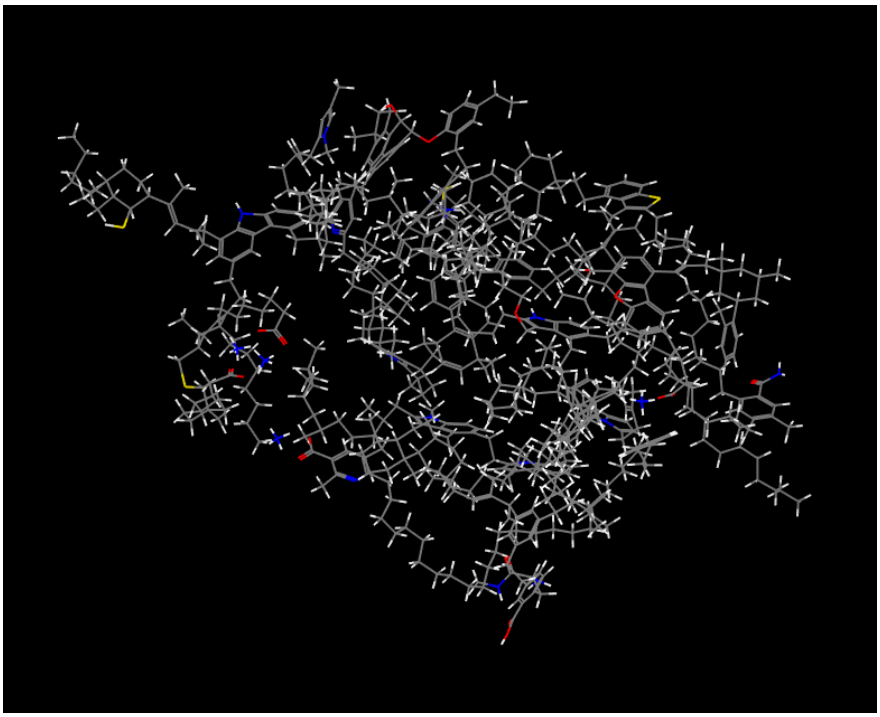

Figure 4.26 The 3D structures of kerogen nanoclusters formed by the adsorption sequence of 1657432.

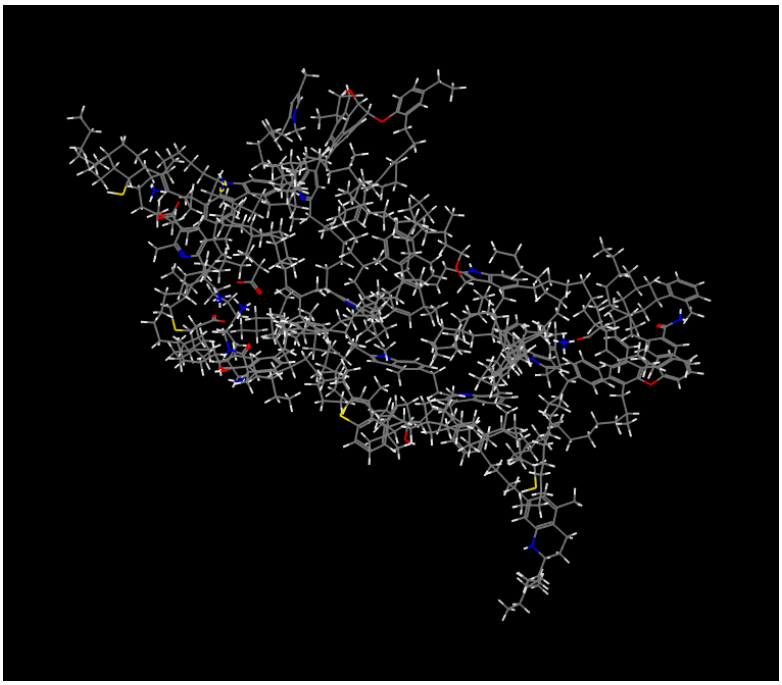

Figure 4.27. The 3D structures of kerogen nanoclusters formed by the adsorption sequence of 1257436.

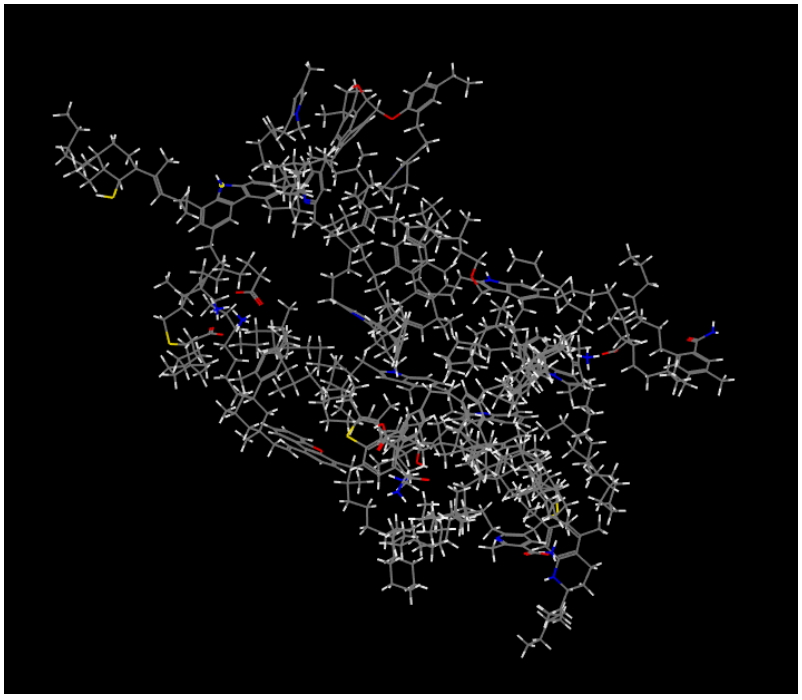

Figure 4.28 The 3D structures of kerogen nanoclusters formed by the adsorption sequence of 1263547.

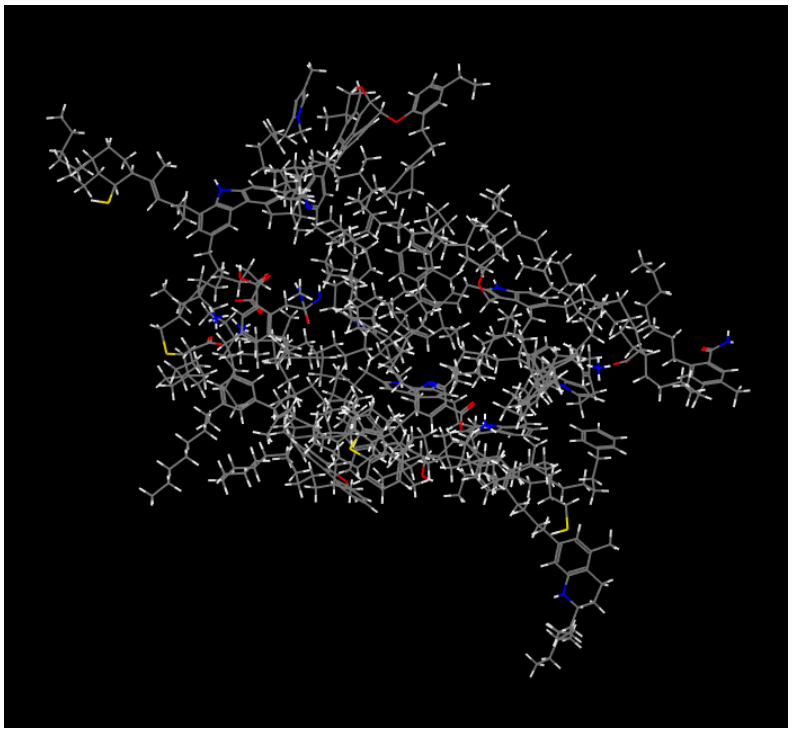

Figure 4.29 The 3D structures of kerogen nanoclusters formed by the adsorption sequence of 1273645.

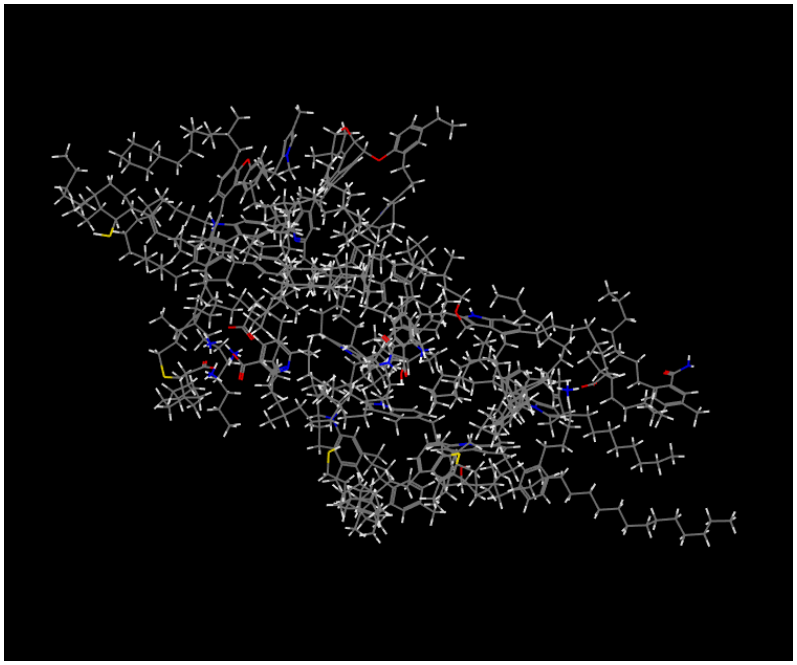

Figure 4.30 The 3D structures of kerogen nanoclusters formed by the adsorption sequence of 1457263.

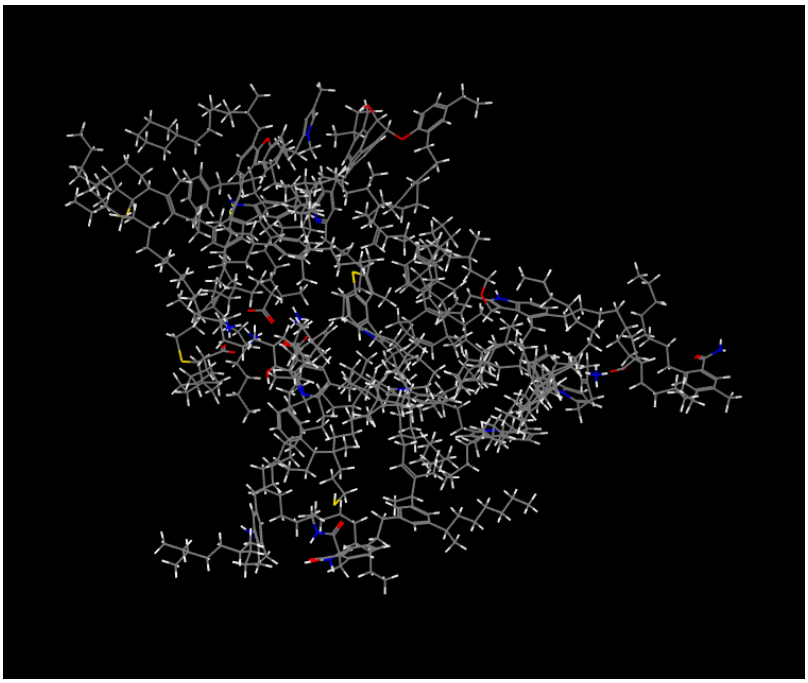

Figure 4.31 The 3D structures of kerogen nanoclusters formed by the adsorption sequence of 1463527.

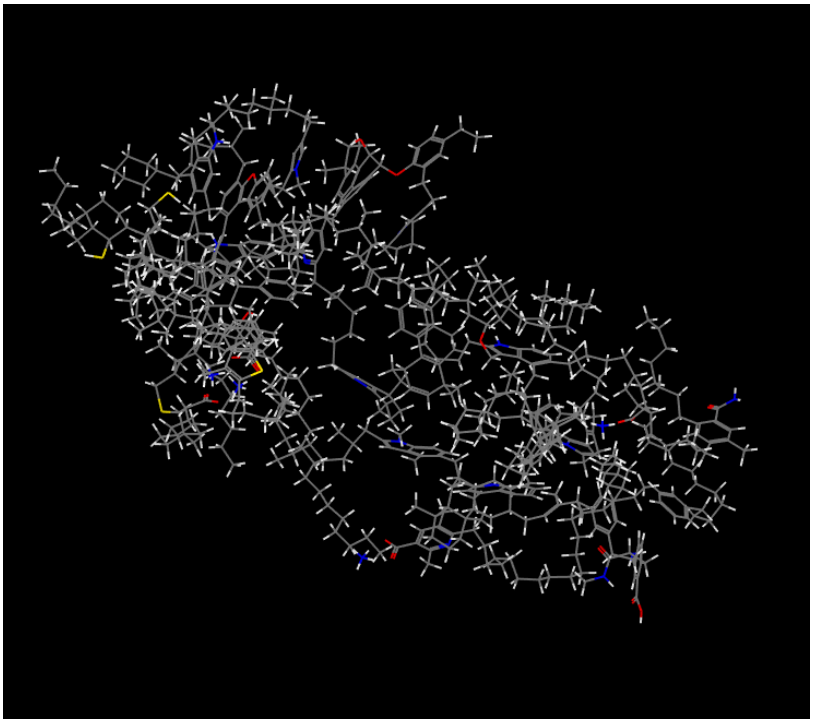

Figure 4.32 The 3D structures of kerogen nanoclusters formed by the adsorption sequence of 1473625.

Table 4.1 The released adsorption energy from adsorption of group II molecules on molecule 1 and group III molecules on the configuration with lowest energy state (1243) obtained from the first step.

Sequence	1234	1243	1324	1342	1423	1432
E_{ads} (Kcal/mol)	-717.14	-724.12	-721.71	-716.74	-715.72	-716.38

Sequence	1243567	1243576	1243657	1243675	1243765	1243756
E_{ads} (Kcal/mol)	-962.58	-953.30	-952.22	-950.75	-944.86	-945.48

Table 4.2 The released adsorption energy from adsorption of group III molecules on the configuration with the second lowest energy state (1324) obtained from the first step in Table 1.

Sequence	1324567	1324576	1324657	1324675	1324765	1324756
E_{ads} (Kcal/mol)	-951.42	-945.73	-947.22	-952.59	-948.45	-948.85

Table 4.3 The released adsorption energy from adsorption of group III molecules on molecule 1 and group II molecules on the configuration with the lowest energy state (1657) obtained from the first step.

Sequence	1567	1576	1657	1675	1756	1765
E_{ads} (Kcal/mol)	-223.597	-223.798	-228.357	-226.829	-224.955	-228.332

Sequence	1657234	1657243	1657324	1657342	1657432	1657423
E_{ads} (Kcal/mol)	-939.32	-936.24	-944.25	-943.70	-929.89	-935.41

Table 4.4 The released adsorption energy from alternative adsorption of groups II and III molecules on molecule 1.

Sequence	1273645	1263547	1257436	1473625	1463527	1457263
E_{ads} (Kcal/mol)	-945.71	-938.79	-931.14	-933.97	-931.60	-954.04

To further confirm our assumption, we studied the adsorption processes in the other three patterns. In the proposed procedure, the sequence releasing the most adsorption energy in the first step was applied to the second step. Here we further applied the sequence with the second lowest energy in step I to construct 6 kerogen models through step II. The results are shown in Fig. 4.15-4.20 and Table 4.2. As expected, the adsorption energy released in this pattern in Table 4.2 is lower than that of the sequence of 1243567 which validated our assumption.

In the second pattern, we first threw the small molecules from group III into the matrix. Then with the sequence with the lowest energy state in the first step, we further added the large molecules of group II into the model. The results are shown in Fig. 4.21-4.26 and Table 4.3. Obviously, the adsorption energy of each sequence in this group is less than that of the sequence 1243567 which corroborates our assumption.

In the third pattern, the molecules in group II and III were added into the matrix in an alternative pattern. Six sequences were examined and the results are shown in Fig. 4.27-4.32 and Table 4.4. It can be seen that the adsorption energy of the each sequence in this group is less than that of the sequence 1243567. This result substantiates our idea.

Therefore, the adsorption energy of the total 24 sequences in four patterns is computed and the kerogen model releasing the most energy with the sequence of 1243567 was obtained in the proposed pattern that provides positive support to the designed procedure.

4.1.4 The Solid State Model of Kerogen

In the previous section, an adsorption-based method is developed to build the kerogen nanocluster model. However, such a nanocluster model is still quite different from the structure of a real kerogen[12-14]. As discussed above, a real kerogen is always under a certain pressure while the nanocluster model is in fact built in vacuum. Moreover, a real kerogen is a bulk solid state material not a nanocluster. The difficulty in building a solid state kerogen model lies in the fact that kerogen is a kind of amorphous material. Lack of regular patterns in amorphous materials, a real kerogen model means a model as large as the kerogen sample itself. For a 1 mg sample, there will be around 10^{18} to 10^{19} atoms in the model that is far beyond current computation capabilities. However, a rational solid state kerogen model is vital to understand and predict the properties of kerogen and highly desired in current shale oil/gas research. Here we propose a strategy to mimic the amorphous kerogen by building a crystal counterpart of kerogen. The crystal counterpart has the same average composition with amorphous kerogen. But with the information of one unit cell, the properties of the bulk kerogen can be calculated. Moreover, a kerogen structure under a certain pressure can be obtained that is more realistic than the nanocluster model. Currently this method seems to be the only viable way to building a bulk solid state model of kerogen. It should be noted the similar strategies have been implicitly applied in kerogen research widely. For example,

the molecule structure shown in Fig. 4.1 was proposed by Siskin et al.[8] to represent the composition of kerogen. However, as an amorphous material, there should be no regular units in kerogen. Therefore, even with the same atoms, the 2D molecular structure of other parts of kerogen could be different from the structure shown in Fig. 4.1. But statistically this structure can be viewed as an average structure that represents the kerogen 2D molecular structure. Later on, Orendt et al.[14] built a 3D nanocluster model of kerogen. They further calculated the NMR and atomic pair distribution function (PDF) of this kerogen model and found the theoretical results matched the experimental data very well. When they compared their calculation results with the experimental ones, they implicitly considered the other parts of the kerogen being composed repeatedly of the same nanocluster. Therefore, from the analysis of previous work, we can come to the following conclusions:

1. Due to the amorphous nature of kerogen, it is impossible to establish the strict composition and structure model of kerogen. Therefore, it is a general strategy to use a typical unit to represent the composition/structure of whole kerogen and consider the whole kerogen being made up by this unit repeatedly.

2. Based on the comparison of experimental and theoretical results, it can be confirmed that for some properties, such as NMR and PDF, this strategy is valid as proved by Orendt et al. It can be concluded that although the composition and structure of kerogen vary everywhere, some properties of kerogen can be calculated in a tolerable error range by assuming the kerogen is made up by an average structure unit repeatedly.

In this work, we extend this strategy to build an average 3D unit cell for kerogen. Similar to previous work, this is a kind of simplified but effective treatment to the complicated kerogen structure and may provide a novel powerful tool for kerogen research. As will be shown below, with this method, the solid state kerogen model under a certain pressure can be established and the calculated properties of this solid state kerogen model agree with experimental results very well.

The procedure to transfer the nanocluster model to a crystal structure model is described as below:

1. A cubic unit cell (60Å×60Å×60Å) large enough to hold the whole kerogen molecular nanocluster was built and the nanocluster was put inside this unit cell as shown in Fig. 4.33a.

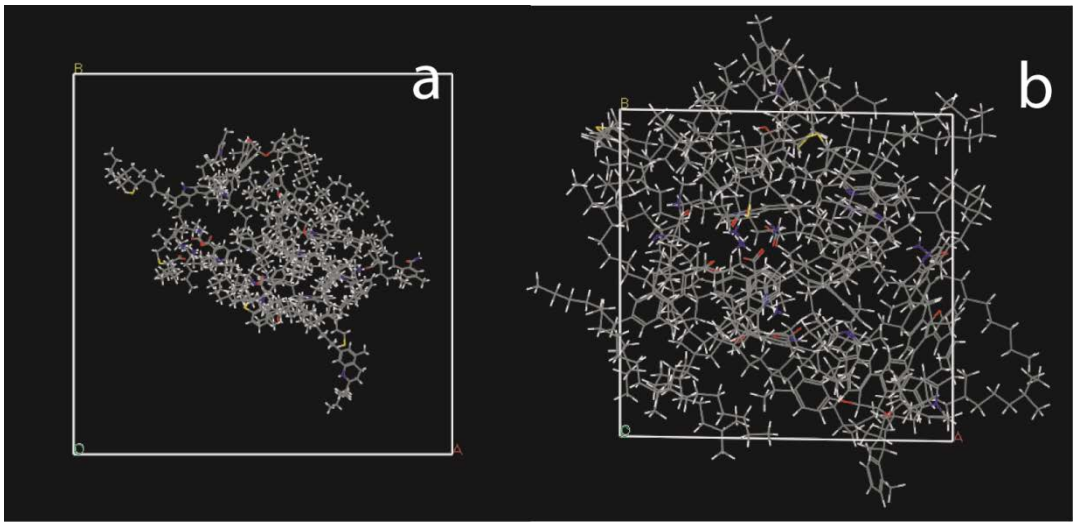

2.

Figure 4.33 a. The kerogen nanocluster with the sequence of 1243567 in a big unit cell (a=b=c=60Å, α=β=γ=90o). b. the kerogen nanocluster in the unit cell after MD simulation (a=24.96Å, b=24.49Å, c=26.58Å, α=94.17^o, β=93.19^o, γ=90.65^o).

2. Molecular dynamics simulation was applied to build the solid state model of kerogen. Firstly, the cell was subjected to a 2 ns NVT MD simulation at 298K which was followed by a 6 ns NPT simulation at 10^5 Pa (1 atm) and 298K using a Berendsen weak coupling method to control pressure. Then a 6 ns NPT simulation was conducted with Parrinello-Rahman pressure coupling. Finally a 30 ns NVT was conducted. The Nose-Hoover thermostat was applied to maintain the temperature at 298K and the pressure coupling was carried out with relaxation times of 100fs and 1000 fs for Berendsen and Parrinello-Rahman methods respectively. The time step of all the simulation was 1fs. Criteria for equilibrium included constant values of average pressure, temperature, energy and density profiles for the kerogen model.

Through MD simulation, the solid state kerogen model under 1 atm at 298K was built and shown in Fig. 4.33b. As discussed above, this solid state model under a certain pressure and temperature is closer to the real kerogen than the molecular nanocluster model and the calculation of many properties of solid state materials becomes possible with this new model. For example, the density of the kerogen was calculated to be 0.968 g/cm^3. This result is reasonable considering the fact that the density of kerogen ranges from 0.95 to 1.5 g/cm^3 depending on the maturity[17]. Moreover, the mechanical properties of kerogen were calculated as discussed in the following.

4.2 Properties Calculation of Kerogen based on the 3D Model

4.2.1 Mechanical Properties of Kerogen

The mechanical properties of kerogen were calculated with the Forcite module of Materials Studio 7.0 using the constant strain approach. To keep the structure within the linear elasticity region while avoiding that the strains were too low and computational noise might become significant, the maximum strain amplitude was set to 0.003 and 4 distorted structures were generated for each strain pattern. The amorphous kerogen is considered as isotropic materials that the stress-strain relations can be completely described by two parameters: Lamé constants λ and μ. The Young's modulus E, Poisson ratio ν, bulk modulus K and shear modulus G can be calculated using the following formula[16]:

$$E = \mu\left(\frac{3\lambda + 2\mu}{\lambda + \mu}\right), \quad \nu = \frac{\lambda}{2(\lambda + \mu)}, \quad K = \lambda + \frac{2}{3}\mu, \quad G = \mu$$

With the 3D solid state model of kerogen built above, the following results were obtained:

λ= 1.72GPa,	μ=1.37GPa,	E=3.50GPa,
ν=0.25,	K=2.63GPa,	G=1.37GPa.

In addition, the compressibility of kerogen was calculated as 370.64 TPa^{-1}.

Zeszotarsky et al.[18] measured the mechanical properties of the Woodford shale kerogen isolated from matrix by dissolving rock. The Young's moduli were 10.5 to 11.1 GPa. However, the kerogen might alter during the isolation process. Mba et al.[19] studied the mechanical properties of Bakken shale samples with the nano-indentation technique and observed a Young's moduli ranging from about 15GPa to 25 GPa. However, it was not indicated whether the target is kerogen, clay or some other minerals. Recently, Kumar et al.[20] measured the Young's modulus of kerogen samples

from Woodford shale play based on the nano-indentation method. Without an isolation process, they found Young's modulus of kerogen was dependent on localized porosity and maturity and the Young's moduli of samples ranged from 1.9 to 15 GPa. While the measured Young's modulus is dependent on the experimental conditions and sample sources, our result (3.50GPa) of Green River kerogen is comparable to previous experimental results reported by Kumar et al.[20].

Yan et al.[21] measured the bulk modulus of the type I Green River kerogen and the values were around 3.5-5 GPa which are very close to our calculation result of 2.63 GPa. They also concluded that the shear modulus of the kerogen was about half of its bulk modulus, consistent with our calculation results. The calculated shear modulus 1.37 GPa is just about half of the bulk modulus 2.63GPa. Therefore, our theoretical results based on proposed 3D solid state kerogen model are consistent with the experimental ones very well.

4.2.2 The NMR Spectra of Kerogen

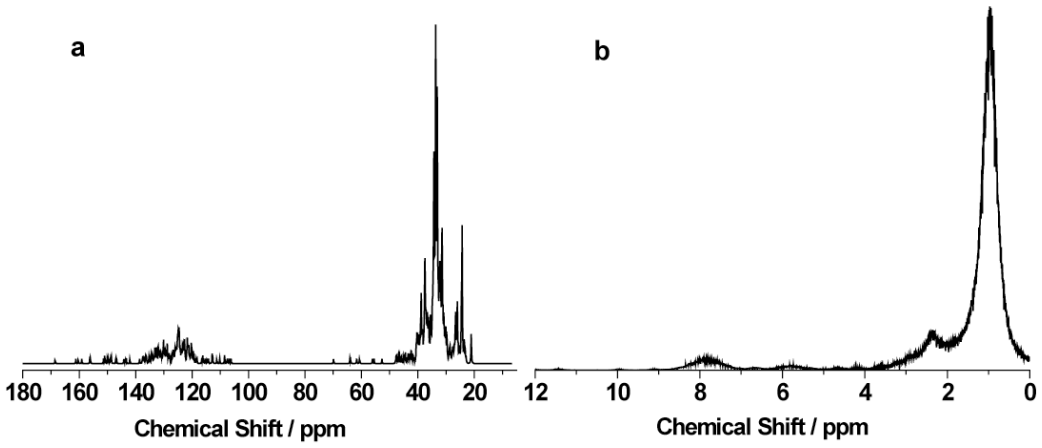

Figure 4.34 ^{13}C(a) and ^{1}H(b) NMR spectra of the solid state model of kerogen.

With the 3D solid state model of kerogen, all the IR, Raman, ^{13}C NMR and ^{1}H NMR spectra of kerogen can be calculated.

Due to its insoluble nature in solvents, solid state NMR has become one of the most important tools to characterize and study the chemical structure of kerogen. Premović et al.[22] studied the solid state NMR of Green River kerogen. Due to the limitation of resolution and structural complexity of kerogen, they found two broad peaks at 24 and 125 ppm in ^{13}C NMR spectra. The widths of the peaks were 20 and 40 ppm respectively. The first peak was assigned as aliphatic carbon and the second one arose from aromatic/alkenic carbon. These results are consistent with other reports[23, 24] that there were two broad peaks in kerogen ^{13}C NMR spectra. The one ranging from 20 to 80 ppm was assigned to aliphatic carbons while the other ranging from 80-160 ppm was assigned to aromatic/alkenic carbons.

After geometry optimization, the ^{13}C NMR and ^{1}H NMR spectra of the obtained kerogen model were computed at the Restricted Hartree–Fock level of theory using the minimal STO-3G basis set. The calculated chemical shielding values were converted to chemical shifts on the tetramethylsilane (TMS) scale (^{13}C at 249.4186 ppm and ^{1}H at 33.7486ppm) and the results are shown in Fig. 4.34. Our theoretical results about ^{13}C NMR spectrum of kerogen agree with the reported experimental data very well. There are two peak clusters as shown in Fig. 4.34a. The first one ranges from 20 to 50 ppm arising from aliphatic carbons while the second one mainly ranges from 110 to 150 ppm arising from aromatic/alkenic carbons.

Premović et al.[22] also found two broad peaks in the ^{1}H NMR spectrum of Green River kerogen. The peak at about 1ppm was assigned to aliphatic protons while the peak at about 8 ppm was assigned to aromatic/alkenic protons. The two peaks were so broad that they overlapped each other. In our calculated ^{1}H NMR spectrum, there are three peaks as shown in Fig. 4.34b. The highest peak at 0.97 ppm and its shoulder peak at 2.35ppm are assigned to aliphatic protons and the peak at 7.85 ppm is assigned to aromatic/alkenic protons. Therefore, both the calculated ^{13}C and ^{1}H NMR spectra match the experimental results very well.

4.2.3 The IR and Raman Spectra of Kerogen

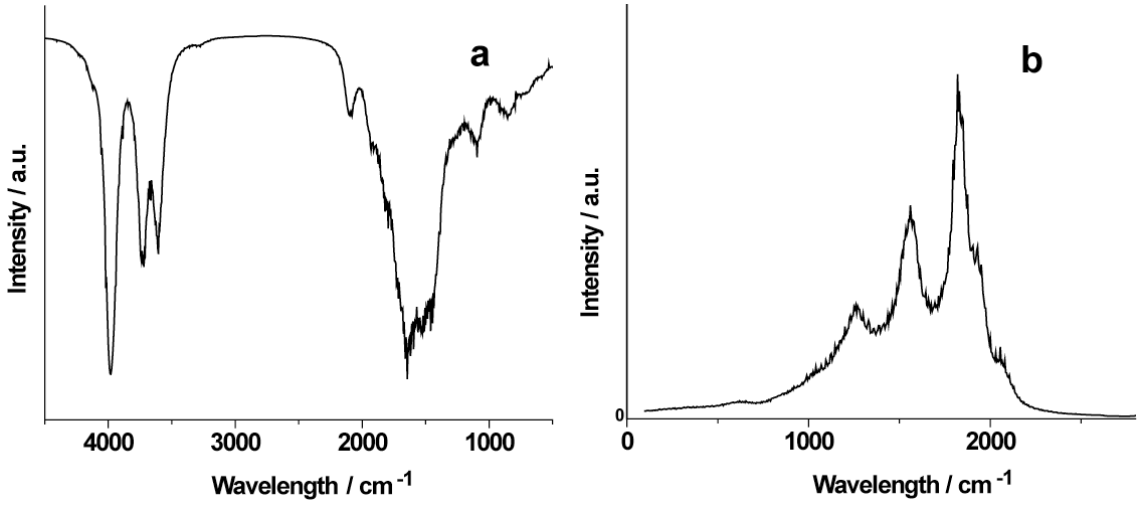

Figure 4.35 IR(a) and Raman(b) spectra of the solid state model of kerogen.

Similar to NMR spectra, after geometry optimization, the IR and Ramam spectra were calculated and the results are shown in Fig. 4.35a and b respectively. IR and Raman spectra have been widely applied to study kerogen. Ganz et al.[25] proposed to define the maturation level of kerogen based on IR. Zeng et al.[26] studied the thermal decomposition process of kerogen coupling IR and Raman spectra. Robinson[27]

reported the IR spectrum of Green River kerogen and the main peaks are listed in Table 5. Althouth better results can be obtained at higher-level theoretical calculations with basis sets such as 4-31G and 6-31G, due to the large size and heavy computational burden of molecule 1, only the minimal basis set STO-3G was applied in our calculation. Therefore, the calculated absolute peak positions are not very accurate but their relative positions are correct. The peaks are also assigned in Table 4.5 and the calculation results agree with the experimental results very well.

Table 4.5 The assignment of peaks in the IR spectrum.

Assignment of IR peaks	**Experimental results / cm^{-1}**	**Calculation results / cm^{-1}**
NH, OH stretching band	2700-3700	3860-4500
CH stretching bands of alkyl groups	2860-2930	3400-3860
C=O stretching band	1710	2095
C=C stretching of olefins, aromatic rings	1630	1310-2025
Asymmetric bending of CH_2 and CH_3	1455	

Raman spectrum is another important technique of characterizing kerogen. It is well accepted that there are two Raman bands in kerogen's Raman spectrum: D-band at 1603nm and G-band at 1354 nm. In the calculated Raman spectra as shown in Fig. 4.35b, there are three peaks related to the C-H vibration modes in aliphatic or aromatic structures. According to the position and intensity of the peaks, the peak at 1820 cm^{-1} is the D-band and the peak at 1560 cm^{-1} should be the G-band. Besides these two peaks, there is also a small peak at 1270 cm^{-1}. Normally Raman spectra are measured from a laser spot with the sizes ranging from 0.5 to 10 μm. Therefore, it only provides the local information from a very small area of the sample. On the other hand, the spectrum

quality is affected by the integration time, resolution of the instrument and other experimental details. Since the theoretical spectrum represents a result that will be obtained under ideal conditions for a specific configuration, the difference between experimental and theoretical calculation is understandable. Therefore, overall the calculation results are in accordance with the experimental data.

Chapter 5: 3D Porous Structure Model of Kerogen and Adsorption Property Calculation

5.1 3D Prous Structure Model of Kerogen

As discussed earlier, after formation, the gas or oil molecules are stored in the pores of shale. Therefore, theoretically the transportation and storage of these molecules should be determined by their interaction with the pore well of kerogen. Recent experimental studies also indicate that the pores in organic matter (kerogen) are a significant component of the total pore system in gas shales and most of the storage capacity in gas shales is contributed by these organic pores in kerogen. It has been revealed that greater gas adsorption capacity of shale is obtained from samples with higher total organic carbon (TOC) content[28,29]. Moreover, the amount of adsorbed gas could account for up to 85% (Lewis Shale, USA) of total gas initial in-place. Both theoretical and experimental studies imply that the recovery of shale gas is essentially a process to release the adsorbed gas from kerogen. Currently, one main issue with shale oil production is the low primary recovery factors still less than 10%. There is no doubt that it is vital for petroleum engineers to elucidate the mechanism of interaction (absorption) between hydrocarbon molecules with kerogen pores as the indispensable theoretical basis to scientifically design new methods to enhance the recovery of shale gas reservoirs.

As the first step to achieve this goal, the structure of the organic pores in kerogen must be clarified. Therefore, recently great attention has been paid to study the structure, distribution and properties of these organic pores experimentally[30, 31]. However, there

is still few information about the atomic-level structure of kerogen pores. Recently, the adsorption and transportation of hydrocarbons have been studied by molecular dynamics simulation[32,33], however, the pore or slit models in these reports are carbon nanotube or 2D carbon sheet with smooth surface and pore wells which is physically and chemically much different from real kerogen. In fact, with the development of modern computational chemistry, the methods to calculate the adsorption and transportation of hydrocarbons in nanopores/slits have been well developed. The key difficulty is how to establish a reasonable porous kerogen model.

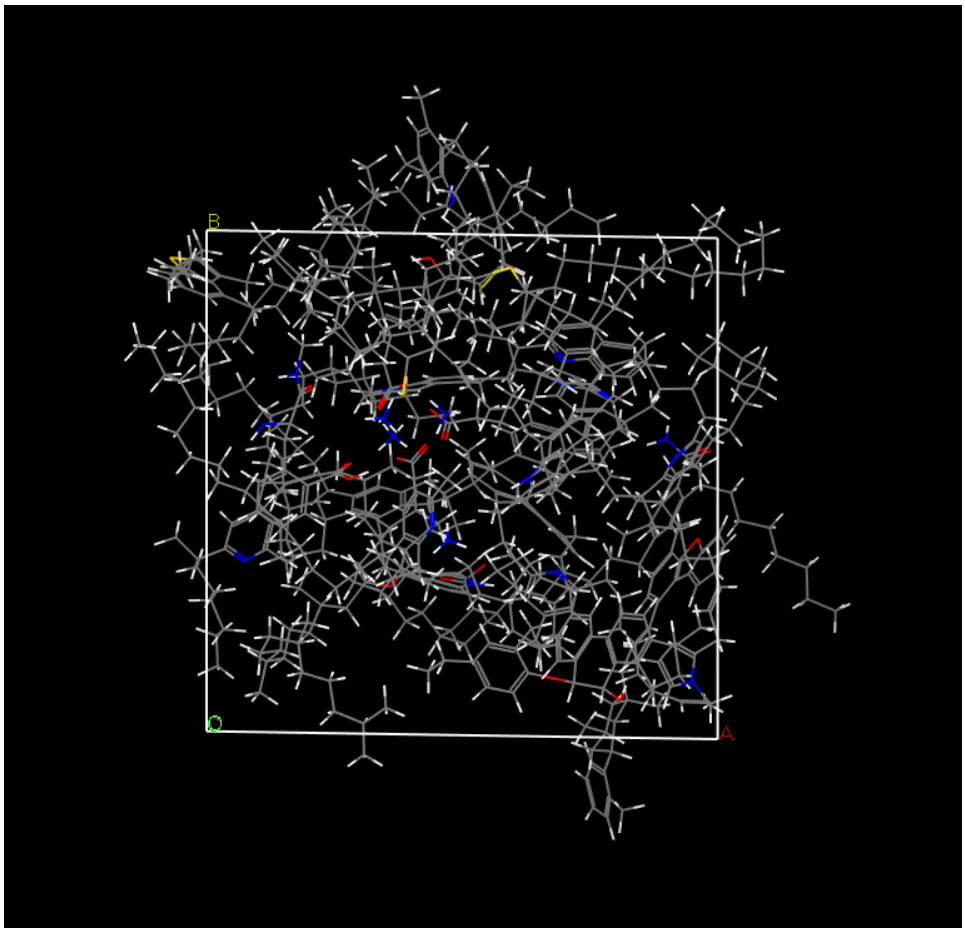

Figure 5.1 The 3D structure of the proposed porous kerogen model.

A kerogen model has been established in the previous chapter. Here I further propose a method to establish a porous kerogen model based on oil/gas formation mechanism. As discussed in the literature review, buried in sand/mud, the biopolymers will decompose into small compounds. These compounds undergo new condensation reactions and produce fulvic acids and humic substances which become progressively insoluble due to increasing polycondensation and finally result in kerogen. Consecutive deposition of sediments induces burial of previous beds deeper, the equilibrium established at the end of diagenesis to form kerogen is broken by the increasing temperature and pressure. During catagenesis process, small molecules continue to be generated as the result of kerogen decomposition. Black oil, volatile oil, condensate, wet gas and dry gas are produced in sequence at higher temperature. Obviously, under the ground, there is no void space or pores in kerogen. Originally, kerogen is composed of large polymers that occupy all the space. After the large polymers break down, the produced small molecules will occupy all the space with the left large polymer fragments together. For the purpose of the experimental study, core samples are taken out of underground. During this process, the small molecules will leave the sample. For example, under atmosphere pressure and room temperature, small molecules such as methane and ethane, are gases and will easily diffuse into the air. Some other molecules, such as hexane, heptane, are liquids at room temperature. But they may also leave kerogen due to their volatility. After the leaving of these small molecules, pores will form at the space they occupied before which are studied and characterized in the labs. Therefore, from a chemistry perspective, the pores in kerogen are essentially the space used to

contain the small molecules. To match this pore formation mechanism, the best way to build porous kerogen model is to delete the small molecules from kerogen model.

There are totally seven molecules in the Siskin's 2D molecular structure of Green River oil shale kerogen. Molecule 1 ($C_{366}H_{559}O_{10}N_{13}S_2$), 2 ($C_{102}H_{167}ONS_2$), 3 ($C_{75}H_{121}O_5N_5$) and 4 ($C_{45}H_{60}O$) are very large while molecule 5 ($C_{20}H_{42}$), 6 ($C_{18}H_{30}$) and 7 ($C_{18}H_{38}$) are small molecules that are either liquid at room temperature or highly soluble in organic solvents. Therefore, here a simple but reasonable method to build porous kerogen model is proposed by deleting molecule 5, 6 and 7 from the solid state kerogen model. The obtained porous kerogen model is shown in Fig. 5.1.

5.2 Theoretical Calculation of the Isotherms on Kerogen

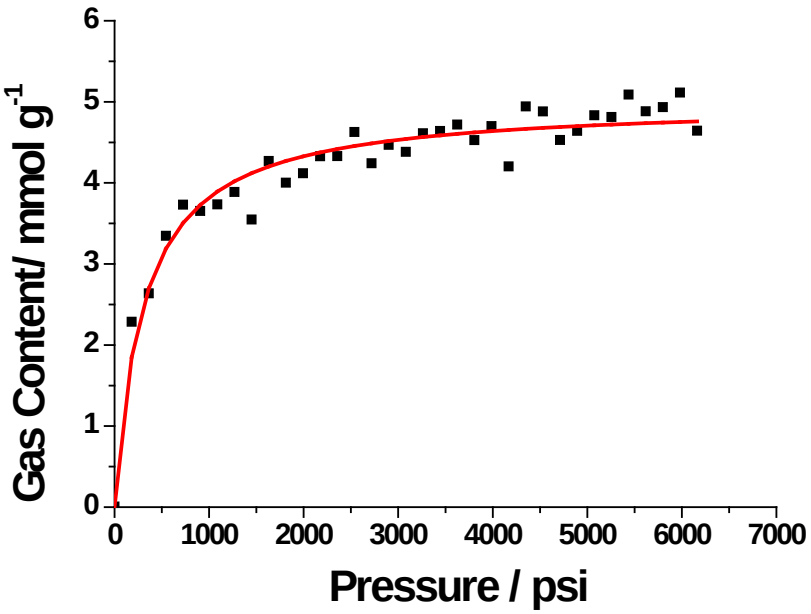

Figure 5.2 Adsorption of methane on porous kerogen at 77°F

To validate the proposed method and justify the porous kerogen model, the adsorption isotherms of methane on the porous kerogen model was calculated at room temperature (77^{o}F) based on the Metropolis Monte Carlo method. Currently, several models, such as Langmuir model and BET model have been proposed to describe the adsorption of hydrocarbon molecules on shale samples[28]. Here, Langmuir model is examined to fit the theoretical results of the adsorption isotherms.

$$V(p) = \frac{V_L P}{P + P_L}$$

V(p) is the gas content of absorption at pressure p; V_L is termed as Langmuir volume, the maximum adsorption of gas at the infinite pressure; P_L is the pressure at which the adsorption is half of V_L.

As shown in Fig. 5.2, the adsorption isotherm matches the Langmuir model very well for methane up to 6000 psi. Therefore, our results indicate that Langmuir model is valid in describing the adsorption of hydrocarbons (up to six carbons) in shale up to 6000 psi. The Langmuir pressure P_L of methane on our porous kerogen model is 309 psi and the Langmuir volume is 3953 scf/ton (4.997mmol/g). To the best of our knowledge, there are very few reports about the adsorption isotherm of hydrocarbon molecules on Green River oil shale kerogen. However, isothermal adsorption of methane gas on other shale has been measured experimentally[34,36]. It was reported that the measured data matched best with the BET models that is consistent with our results. The P_L of the samples ranged from 143 to 1145 psi and the V_L was between the 30 to 959 scf/ton. Obviously, the Langmuir pressure of our results is in the same order of experimental results but the calculated Langmuir volume is too large. This is because the calculated Langmuir

volume is for pure kerogen but the experiments were conducted with shale which is a mixture of kerogen and inorganic component. Suppose the organic matter in the sample is kerogen that only accounts for 5% of total weight of shale and all the adsorption in the shale is on kerogen, then the V_L of the theoretical results will be 198 scf/ton. Therefore, our calculation result is comparable to the experimental results. Although these data are measured from other shale but not Green River oil shale, the consistence of our theoretical results with these experimental data shows that our calculation results provide a reasonable estimation of adsorption properties of shale.

Normally, methane adsorption isotherms are measured under room temperature or lower temperatures. While the temperatures of shale gas reservoir could be as high as 335^{o}F at Eagle Ford and 340^{o}F at Haynesville, adsorption measurement at such high temperatures are rare. However, the adsorption parameters are indispensable for accurate simulation of these shale gas reservoirs. Here, we show that such parameters can be obtained feasibly using our theoretical calculation method. As shown above, that adsorption isotherm of methane at room temperature was obtained based on the Metropolis Monte Carlo method which matched the experimental results very well and proved the validity of the method. We further extended the same strategy to calculate the adsorption isotherms of hydrocarbons at higher temperatures as an example to show the advantage of our method since these data were not available experimentally. The adsorption isotherms of six alkanes: methane, ethane, butane, propane, n-butane, n-pentane and hexane, on kerogen were calculated at 212^{o}F. As shown from Fig. 5.3 to 5.8, the adsorption isotherm matches the Langmuir models very well for all six kinds of hydrocarbons up to 6000 psi which is consistent with previous reports. Moreover, with

these data, we obtained an empirical equation to relate the parameters for Langmuir model with the length of hydrocarbon molecules as shown in Figure 5.9 and 5.10.

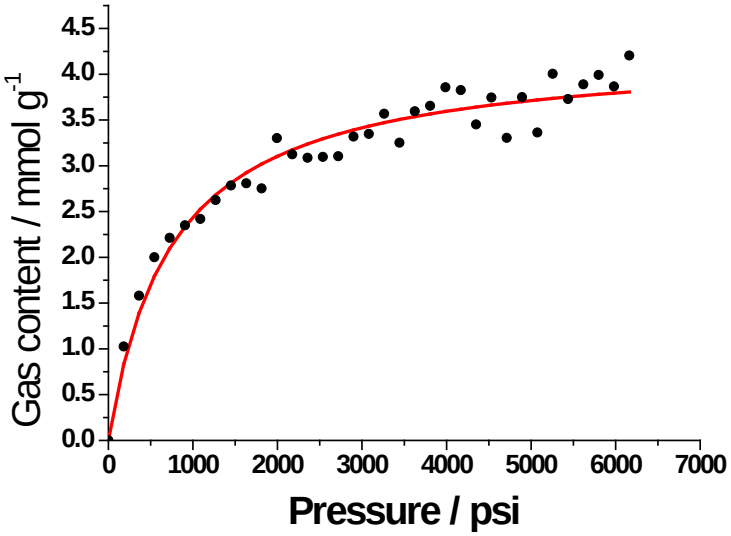

Figure 5.3 Adsorption of methane on porous kerogen at 212°F

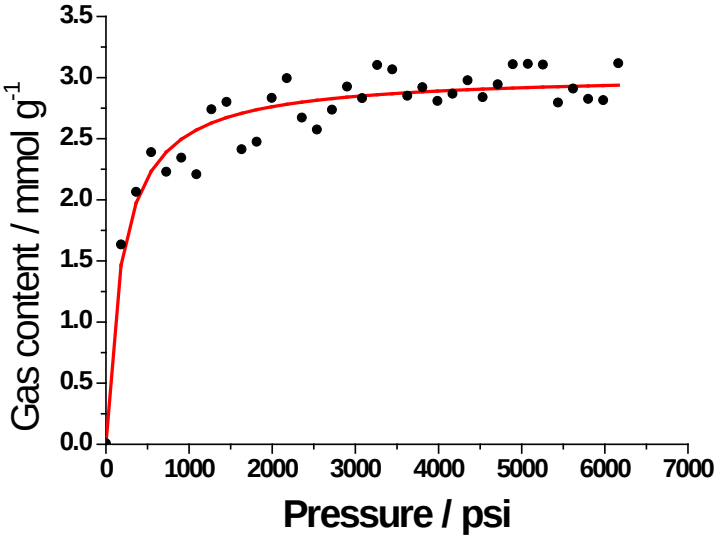

Figure 5.4 Adsorption of ethane on porous kerogen at 212°F

c2

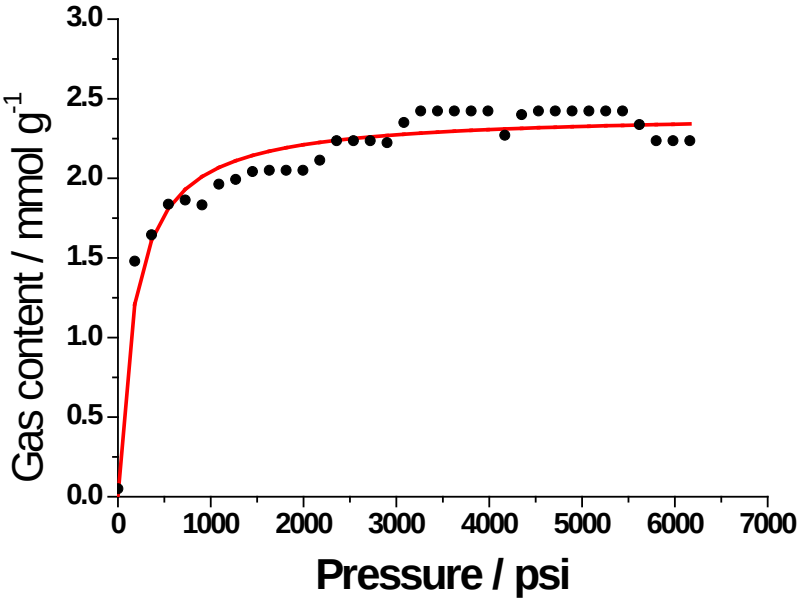

Figure 5.5 Adsorption of propane on porous kerogen at 212°F

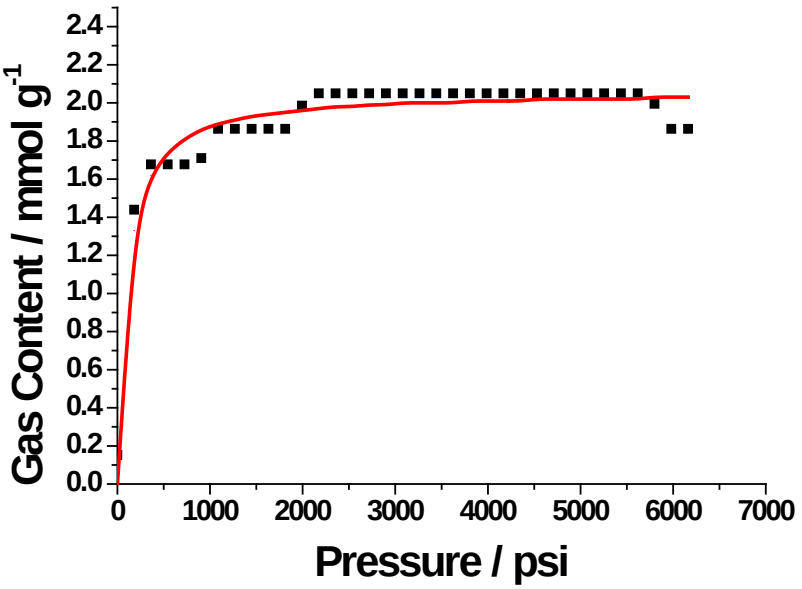

Figure 5.6 Adsorption of n-butane on porous kerogen at 212°F

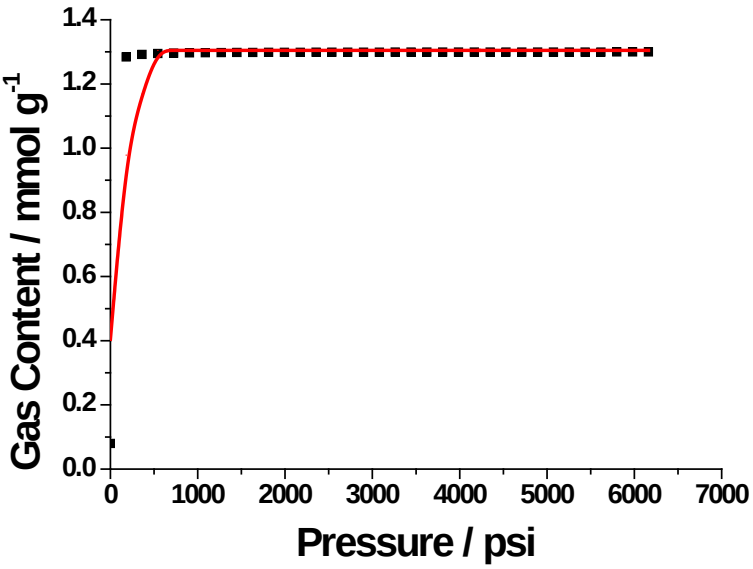

Figure 5.7 Adsorption of pentane on porous kerogen at 212°F

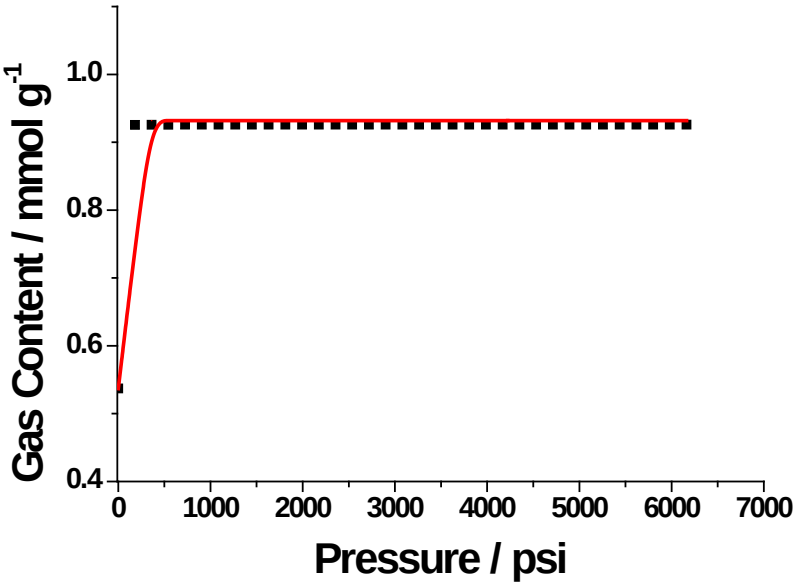

Figure 5.8 Adsorption of hexane on porous kerogen at 212°F

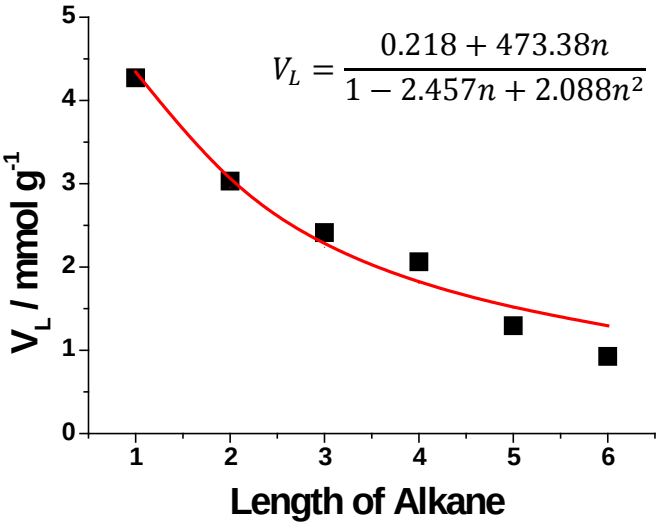

Figure 5.9 Relationship between Langmuir volume V_L and length of the alkanes on the porous kerogen at 212°F (n is the length of the alkane).

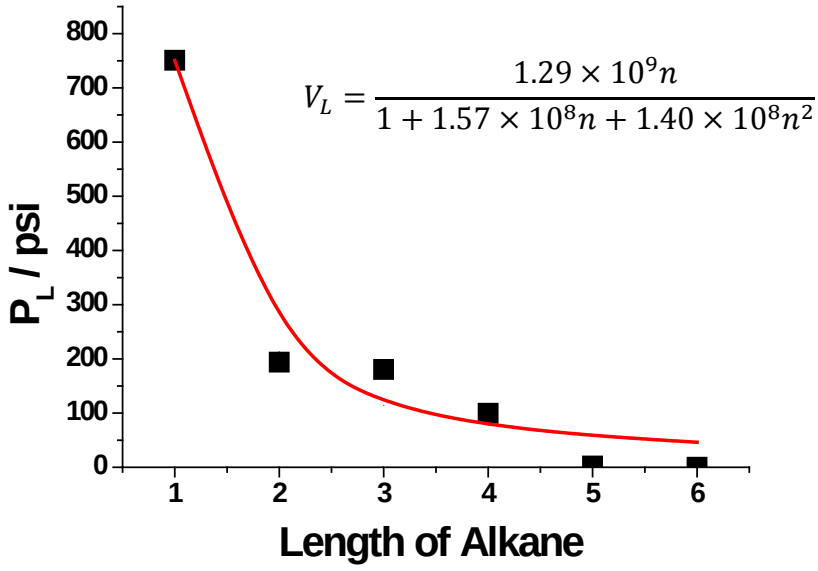

Figure 5.10 Relationship between Langmuir pressure P_L and length of the alkanes on the porous kerogen at 212°F (n is the length of the alkane).

Table 5.1 The parameters to fit the isotherm curves by Langmuir model

Alkane	Gas Content mmol/g	V_L scf/ton	P_L psi	Correlation Coefficient
methane	4.272	3379.365	751.013	0.983
ethane	3.032	2398.283	193.900	0.975
propane	2.414	1909.809	180.335	0.981
butane	2.063	1631.855	99.617	0.986
pentane	1.295	1024.558	2.224	0.974
hexane	0.926	732.8583	0.105	0.983

5.3 Reservoir Simulation Based on the Calculated Isotherms

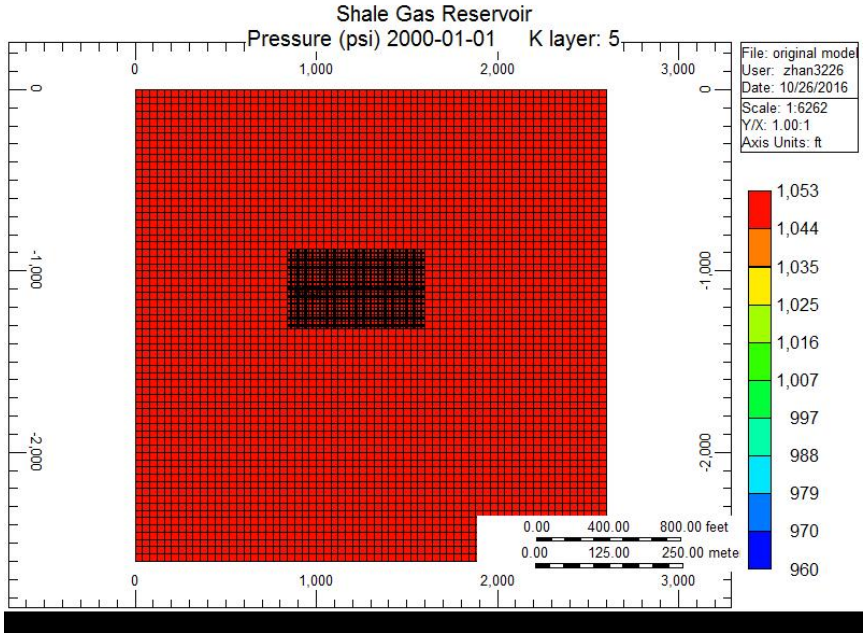

Figure 5.11 The reservoir model for shale gas production simulation. The reservoir dimensions are I: 55×50ft, J: 55×50ft, K: I: 10×30ft. The horizontal well is in the fifth layer with a length of 900 ft.

Although some parameters under reservoir conditions are vital for successful accurate reservoir simulation, they may be not available experimentally. Here based on the proposed method, these parameters can be obtained from theoretical calculation. Based on these parameters, a reservoir simulation is performed to examine the effect of

adsorption on the production of shale gas and it shows the advantage of our method. The reservoir model is shown in Fig.5.11 and the parameters for simulation are shown in Table. 5.2.

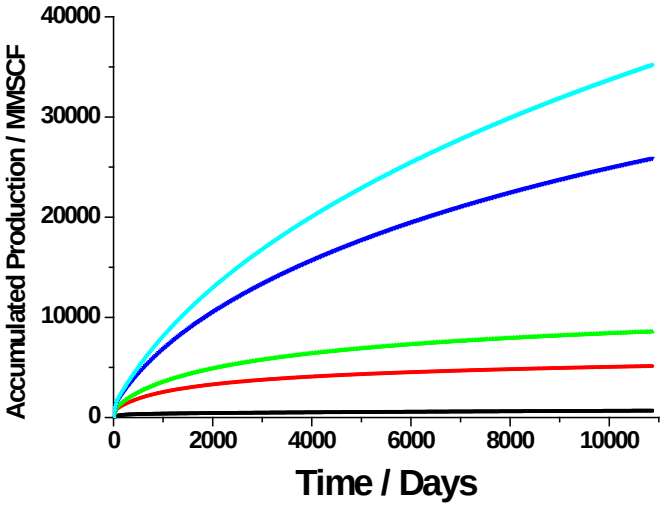

Figure 5.12 Accumulated gas production with different Langmuir volumes (V_L), Cyan(21.69 mol/lb), blue(11.93mol/lb), green(2.169 mol/lb=4.272mmol g^{-1} which is our calculated V_L of methane at 212^{o}F on a shale containing 5% kerogen), red(1.08mol/lb) and black(0 mol/lb).

The simulation results are shown in Fig. 5.12. Obviously, the adsorption parameters have a great impact on the production. For the reservoirs with higher maximum adsorption amount (V_L), more methane is produced because more methane can be released from reservoir. This effect is observed even in a short production period. As shown in Fig. 5.13, even the production at the end of the first year is significantly dependent on the adsorption properties of shale. Therefore, for more reliable reservoir simulation, it is of great importance to acquire the parameters for adsorption as accurate as possible. Since some of these parameters are not available experimentally, our

theoretical calculation method provides a reasonable way to obtain these parameters which represents an excellent case to apply computational chemistry methods to solve the problems in petroleum engineering.

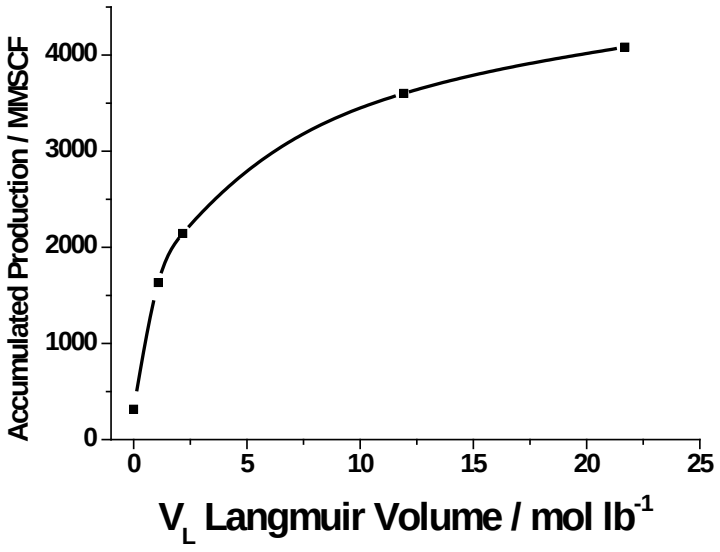

Figure 5.13 The relationship between accumulated gas production at the end of the first year and Langmuir volume(V_L)

Table 5.2 The parameters for reservoir simulation

Parameter	Value	Unit
Length	2750(55×50)	ft
Width	2750(55×50)	ft
Height	300(10×30)	ft
Reservoir temperature	212	^{o}F
Reservoir permeability	100	nD
Reservoir porosity	0.03	
Gas specific gravity	0.3	
Fracture permeability in I, J direction	2×10^{-5}	md
Fracture permeability in K direction	4×10^{-5}	md
Fracture spacing in I, J direction	50	ft
Fracture spacing in K direction	0	ft
Rock compressibility	1×10^{-6}	1/psi
Rock density	120	lb/ft^3
P_L of matrix	751	psi
Grid top	950	ft
Primary fracture width	0.001	ft
Intrinsic permeability	10000	md
Tip permeability	5000	md
Fracture half length	350	ft
Horizontal Well Length	800 (22:40, 28, 5)	ft

Chapter 6: Conclusions and Recommendations

6.1 Conclusions

As the source of gas and oil, kerogen is an indispensable component of shale: the source rock, which plays a key role in determine the mechanical, physical and chemical properties of shale reservoirs. Previously, 3D models of kerogen have been proposed which were essentially single macromolecule models built under vacuum. In this thesis, a solid state model of kerogen was built combining the adsorption calculation and molecular dynamics simulation method. The major progresses achieved in this thesis compared with previous work are summarized as following:

1. Despite of the fact that kerogen is a mixture of multiple molecules, most of previous kerogen models were built based on only one single large macromolecule. In the present thesis, based on an adsorption method, seven molecules were combined together to build one molecular nanocluster model which treated kerogen as a mixture instead of one single macromolecule. Compared with previous models, this new model is more realistic and the proposed method can be generalized to build kerogen models from other shale plays;

2. In most of previous kerogen macromolecular models, there was only one single macromolecule in the model. The materials represented by these models were not real solid state materials. These models were built under vacuum and there were no pressure parameters in these models. In this thesis, based on molecular dynamics simulation method, the molecular nanocluster model built in the first step was further transformed to a solid state model. Pressure was endowed to the kerogen model during molecular

dynamics simulation which means the configuration of the model will vary with pressure. Higher density will be obtained under high pressure which makes our model more realistic;

3. Based on the solid state model of kerogen, the theoretical prediction of the mechanical properties of kerogen become possible. Therefore, to the best of our knowledge, for the first time, the mechanical properties, such as Young's modules, Poisson ratio, bulk modules, shear modules, were calculated theoretically from the 3D kerogen solid state model. Our theoretical results quantitatively matched with previous reported values from experimental measurement very well. Moreover, the calculated IR, Raman, ^{13}C and ^{1}H NMR also matched with results in literatures qualitatively. The differences mainly originated from the simplest basis sets we selected due to the limitation of our computation ability. These results provide positive supports to the proposed methods in this thesis.

4. A porous kerogen model was further proposed based on the formation mechanism of oil/gas. Irregular pore shapes were achieved in this model. Compared with most current MD simulation calculation based on carbon nanotube and carbon nano-slit models with smooth and regular shapes of nanopores/slits, the proposed model represents more typical conditions in kerogen. The theoretical calculations based on our model may provide more accurate and realistic simulation of adsorption and transportation of gas/oil in shales.

5. Based on the porous kerogen model, the adsorption isotherm of methane was calculated based on the Metropolis Monte Carlo method. Our theoretical results

matched with previous reports from experimental measurements very well. Methane adsorption isotherms were best fitted by Langmuir model and the parameters for the Langmuir model were in the reasonable ranges. Previously, most shale gas reservoir simulations were based on the parameters acquired experimentally. However, there are reservoir conditions that the parameters are hard to be measured experimentally due to the limitation of instruments and methods. Our developed theoretical calculation method provides a novel way to obtain the parameters under required conditions efficiently. As an example, the adsorption isotherms of six hydrocarbon molecules on kerogen at 212^{o}F were calculated. These isotherms were best fitted by Langmuir model. Moreover, two empirical equations were derived to relate the parameters in Langmuir model with the length of hydrocarbon molecules.

A 3D solid state model of kerogen is the key to understanding many properties of kerogen and the petroleum generation process. These properties are especially important for unconventional reservoir recovery. The comparison of experimental and theoretical results can help us build better kerogen models while, on the other hand, a better model can help us understand and predict the hydrocarbon generation, migration and adsorption-desorption process in shale plays, develop new strategies for better hydraulic fracturing design and improve the recovery of unconventional reservoirs. Moreover, as proved by this thesis, some important parameters for reservoir simulation and hydraulic fracturing design can be obtained from computation chemistry methods which show a promising future to apply the computation chemistry technique to solve the problems in petroleum industry.

6.2 Future Work Recommendations

1. In this thesis, a 3D solid state kerogen model was built based on the 2D molecular structure model of Green River oil shale kerogen proposed by Siskin et al by proposing a series of strategies to overcome the difficulties in 3D kerogen modeling. A series of theoretical calculation were performed to calculate different physical and mechanical properties of this kerogen. The validity of the proposed strategy was proved by the consistence of theoretical results and experimental data. There are still several other 2D molecular structures of kerogen available. A direct application of proposed strategies is to build the 3D solid state models of these kerogens. The property calculation of these reported structures is not only the best way to show the value of present work but also the best way to further examine the validity of the proposed strategies;

2. There are total 720 possible sequences to combine seven different molecules. In this thesis, due to the limitation of our computation capacity and time, only 24 sequences were examined with their total adsorption energy. Based on some theoretical consideration, we obtained one sequence that was regarded to release the most adsorption energy. This result can be considered as an engineering solution of the problem. Just like reservoir simulation, if we can get accurate information of all the parameters we need underground, theoretical calculation will provide us an exact simulation about the recovery process. However in reality, it is hard to obtain all the parameters underground. Nevertheless with the parameters available, reservoir simulations are performed to provide reasonable support for reservoir management. Although our 3D solid state kerogen model was built on a molecular nanocluster model selected from 24 models, the consistence of the theoretical results obtained with this

model and experimental data provides a positive support in future work in this direction. Given enough computation resources, it is of great interest to calculate the total adsorption energy of all the 720 sequences and strictly prove the proposed strategy to find the best sequence effectively;

3. Hydraulic fracturing is the key technique in shale reservoir recovery. Mechanical properties of shale play a pivotal role in the hydraulic fracturing design. One of the most attractive future extensions of present work is to build a 3D solid state model of shale with both organic kerogen and inorganic components, such as quartz, carbonates and clays. If the mechanical properties of shale can be predicted by computation chemistry methods, it will represent a significant progress in unconventional reservoir research and may provide a powerful way to solve the problems in hydraulic fracturing and simulation of shale reservoirs.

References

[1] van Krevelen, D.W. 1950. Graphical-statistical method for the study of structure and reaction processes of coal. *Fuel* **29:** 269-84.

[2] Burlingame, A. L. and Simoneit, B. R. 1969. High resolution mass spectrometry of Green River formation kerogen oxidations. *Nature* **222**: 741-747.

[3] Djuricic, M., Murphy, R. C., Vitorovic, D. and Biemann, K.1971. Organic acids obtained by alkaline permanganate oxidation of kerogen from the Green River (Colorado) shale. *Geochimica et Cosmochimica Acta* **35**: 1201-1207.

[4] Schmidt-Collerus, J. J. and Prien, C. H. 1974. Investigation of the hydrocarbon structure of kerogen from oil shale of the Green River Formation. *ACS Division Fuel Chemistry* **19** (2): 100-108.

[5] Yen, T. F. **1974.** A new structural model of oil shale kerogen. *ACS Division Fuel Chemistry* **19** (2): 109-114.

[6]Durand, B. 1980. Kerogen: Insoluble Organic Matter From Rocks. Paris: Technip. pp 218-319.

[7] Behar, F., Vandenbroucke, M. 1987. Chemical modeling of kerogens. *Organic Geochemistry* **11** (1): 15-24.

[8] Siskin, M., Scouten, C. G., Rose, K. D., Aczel, D., Colgrove, S. G. and Pabst, R. E. 1995. Detailed structural characterization of the organic material in Rundle Ramsay Crossing and Green River oil shales. In: Snape, C. (Eds.), Composition, Geochemistry and Conversion of Oil Shales Boston: Kluwer Academic, pp143-158.

[9] Lille, U., Heinmaa, I. and Pehk, T. 2003. Molecular model of Estonian Kukersite kerogen evaluated by ^{13}C MAS NMR spectra. *Fuel* **82** (7): 799-804.

[10]Kelemen, S. R. and Siskin, M. 2004. Organic matter models of oil shale revisited. *Preprints /American Chemical Society, Division of Petroleum Chemistry* **49**: 73.

[11]Freund, H., Walters, C. C., Kelemen, S. R., Siskin, M., Gorbaty, M. L., Curry, D. J. and Bence, A. E. 2007. Predicting oil and gas compositional yields via chemical Structure-chemical yield modeling (CS-CYM): part1. concepts and implementation. *Organic Geochemistry* **38** (2): 288-305.

[12] Yen, T. F. 1976. Structural aspects of organic components in oil shales, In: Yen, T. F. and Chilingarian, G. V., (Eds.), Developments in Petroleum Science 5: Oil Shale. Amsterdam: Elsevier, pp144.

[13] Faulon, J. L., Vandenbroucke, M., Drappier, J. M., Behar, F. and Romero, M. 1990. 3D chemical model for geological macromolecules. *Organic Geochemistry* **6** (4-6): 981-993.

[14] Orendt, A. M., Pimienta, I. S. O., Badu, S. R., Solum, M. S., Pugmire, R. J. and Facelli, J. C. 2013. Three-dimensional structure of the Siskin Green River oil shale kerogen model: A comparison between calculated and observed properties. *Energy & Fuels* **27** (2): 702−710.

[15] Lech, A. R. 2001. Molecular Modelling, Principles and Applications Harlow: Pearson Education.

[16]Mo, Y. Z., Zhang, H. and Xu, J. C. 2014. Molecular dynamic simulation of the mechanical properties of PI/SiO_2 nanocomposite based on Materials Studio. *Journal of Chemical and Pharmaceutical Research* **6**(6): 1534-1539.

[17] Schwarzbauer, J. and Jovancicevic, B. 2015. Fossil Matter in the Geosphere. Cham: Springer, pp51.

[18]Zeszotarski, J. C., Chromik, R. R., Vinci, R. P., Messmer, M .C., Michels, R. and Larsen, J. W. 2004. Imaging and mechanical property measurements of kerogen via nano-indentation. *Geochimica et Cosmochimica Acta* **68** (20): 4113-4119.

[19] Mba, K. C. and Prasad, M. 2010. Mineralogy and its contribution to anisotropy and kerogen stiffness variations with maturity in the Bakken shales. SEG extended abstract presented at Annual Meeting, Denver, Colorado, October.

[20] Kumar, V., Curtis M. E., Gupta N., Sondergeld, C. H. and Rai, C. S. 2012. Estimation of elastic properties of organic matter and Woodford shale through nano-indentation measurements. Paper SPE-162778-MS represented at the SPE Canadian Unconventional Resources Conference. Calgary, Canada, October-Novermeber.

[21] Yan, F. Y. and Han, D. H. 2013. Measurement of elastic properties of kerogen. SEG extended abstract presented at Annual Meeting, Houston, Texas, September.

[22]Premović, P. I., Jovanović, Lj. S. and Michel, D. 1992. Solid state ^{13}C and ^{1}H NMR in kerogen research: uncertainty of aromaticity estimation. *Applied Spectroscopy* **46** (11): 1750-1752.

[23]Petsch, S. T., Smernik, R. J., Eglinton, T. I. and Oades, J. M. 2001. A solid state ^{13}C-NMR study of kerogen degradation during black shale weathering. *Geochimica et Cosmochimica Acta* **65** (12):1867-1882.

[24]Kelemen, S. R., Afeworki, M., Gorbaty, M. L., Sansone, M., Kwiatek, P. J., Walters, C. C., Freund, H. and Siskin, M. 2007. Direct characterization of kerogen by X-ray and solid-state ^{13}C nuclear magnetic resonance methods. *Energy & Fuels* **21** (3): 1548-1561.

[25]Ganz, H. H. and Kalkreuth, W. 1991. IR classification of kerogen type, thermal maturation, hydrocarbon potential and lithological characteristics. *Journal of Southeast Asian Earth Sciences* **5** (1-4): 19-28.

[26]Zeng, Y. S. and Wu, C. D. 2007. Raman and Infrared Spectroscopic Study of Kerogen Treated at Elevated Temperatures and Pressures. *Fuel*, **86**(7-8): 1192-1200.

[27]Robinson, W. E. 1969. Kerogen of the Green River formation. In: Eglinton, G. and Murphy, M. T. J. (Eds.), Organic Geochemistry Methods and Results. New York: Springer-Verlag, pp619-637.

[28]Yu, W., Sepehrnoori, K. and Patzek, T. W. 2014. Modeling gas adsorption in Marcellus shale with Langmuir and BET isotherms. Paper SPE 170801 presented at the SPE Annual Technical Conference and Exhibition. Amsterdam, Netherlands, October.

[29] Lu, X., Li, F., and Watson, A. T. 1995. Adsorption measurements in Devoinian shales. *Fuel* **74** (4):599-603.

[30]Wang, C. C., Yao, J., Wu, K. L., Ren, G. X., Sun, H., Yang, Y. F., Gao, Y., Chen, Z. X., 2014. Organic and inorganic pore structure analysis in shale matrix with superposition method. Paper URTeC: 1922283 presented at the Unconventional Resources Technology Conference, Denver, Colorado, August.

[31] Asana, W. and Yucel, A. I. 2014. Permeability of organic-rich shale. Paper SPE 170830 presented at the SPE Annual Technical Conference and Exhibition, Amsterdam, Netherlands, October.

[32] Kazemi, M. and Takbiri-Borujeni, A. 2016. Flow of gases in organic nanocapillary pores of shale: a boundary-driven molecular simulation study. Paper SPE 180246-MS presented at the SPE Western Regional Meeting, Anchorage, Alaska, May.

[33] Kazemi, M. and Takbiri-Borujeni, A. 2016. Flow of gases in slit shaped nanopores of shale: a boundary-driven molecular simulation study. Paper SPE 180246-MS presented at the SPE Low Perm Symposium, Denver, May.

[34]Li, J. C., Zhang, L. H., Chen, Y. L. 2015. Adsorption behavior study of shale gas: models and new combination approach. Paper SPE 176880-MS presented at the SPE Asia Pacific Unconventional Resources Conference and Exhibition, Brisbane, Australia, November.

[35] Zhao, T. Y., Li, X. F., Zhao, H. W., Dou, X. J. 2015. Micro-storage state and adsorption behavoir of shale gas. SPE 178386-MS, Nigeria Annual international conference and exhibition, Lagos, Nigeria, August.

[36] Mengal, S. A. and Wattenbarger, R. A. 2011. Accounting for adsorbed gas in shale gas reservoirs. Paper SPE 141085 presented at the SPE Middle East Oil and Gas show and Conference, Manama, Bahrain, September.